Late Ordovician regional high-pressure metamorphism in Scotland: Caledonian metamorphic climax predated the closure of Iapetus

Thomas Lamont[1], William McCarthy[2], Rob Strachan[3], Nick M W Roberts[4], Tobermory Mackay-Champion[5], Anna Bird[6] and Mike Searle[5]

[1]Department of Geosciences, University of Nevada Las Vegas, 4505 S Maryland Parkway, Las Vegas, NV 89154, USA

[2]School of Earth and Environmental Sciences, University of St Andrews, St Andrews, UK

[3]School of the Environment and Life Sciences, University of Portsmouth, Portsmouth, UK

[4]Geochronology and Tracers Facility, British Geological Survey, Nottingham, UK

[5]Department of Earth Sciences, South Parks Road, University of Oxford, Oxford, UK

[6]Department of Geology, Geography and Environment, University of Hull, Hull, UK

This manuscript has not been peer reviewed – It has been submitted to Earth and Planetary Science Letters

Abstract

We document newly recognised Late Ordovician high-pressure (HP) metamorphism in the Scottish Caledonides. Garnet growth at ca. 455–445 Ma within metabasic rocks from the Ross of Mull is constrained to pressures >0.9 GPa and was associated with formation of kyanite-bearing assemblages in meta-pelites that equilibrated at peak conditions of 1.0–1.2 GPa and 700–780°C. This requires the burial of rock to ~40 km depth driven by crustal shortening and thickening that *post-dated* Late Cambrian-Early Ordovician Grampian arc-continent collision but *predated* the final Silurian closure of the Iapetus Ocean, south of the Midland Valley. Similar garnet bearing amphibolites dated at ca. 455–445 Ma on the Scottish north coast and Shetland, suggest that this period of HP metamorphism was a regional feature across the Northern Highland Terrane and Shetland. This was followed by Scandian nappe stacking and lower pressure metamorphism at ca. 444–415 Ma, potentially forming a single protracted orogenic phase prior to the final closure of Iapetus. There are several potential drivers for this Late Ordovician event including: (1) subduction flip south of the Midland Valley Terrane to NW-directed subduction followed by collision of cryptic outboard terranes and/or Baltica, (2) continued SE directed subduction and collision of the Midland Valley terrane with Laurentia, or (3) subduction-flip followed by NW-directed flat slab subduction causing protracted accretionary orogenesis. Irrespective of the preferred tectonic model, the climax of Caledonian orogenesis in Scotland predated terminal continental collision.

Introduction

Regional high-pressure (HP) metamorphic events result from deep burial and heating of continental crust during orogenesis (e.g. Weller et al. 2021 and references therein). Multiple HP events may occur within a single orogenic belt due to episodes of terrane collision and/or changes in subduction geodynamics (e.g. Yonkee & Weil 2015 and references therein). However, if accretionary orogenesis is terminated by continental collision, the relative contributions of these tectonic processes to orogenic development may be difficult to ascertain in ancient examples.

The Scottish Caledonides are widely regarded as having resulted from the closure of the Lower Palaeozoic Iapetus Ocean and the collision of Laurentia, Baltica and Avalonia (Fig. 1; Pickering et al. 1988; Soper et al. 1992). They are separated from the Hebridean (Laurentian) foreland to the northwest by the ca. 430 Ma Moine Thrust Zone (Fig. 2). To the southeast, the Northern Highland (NHT) and Grampian (GT) terranes are dominated by Laurentian metasedimentary rocks and are separated by the sinistral Great Glen Fault (GGF). The Midland Valley Terrane is a Cambrian-Ordovician magmatic arc (the Grampian-Taconic arc), and immediately to the south, the Southern Uplands Terrane is an accretionary prism separated from Avalonia by the Iapetus Suture (Fig. 1; Chew & Strachan 2014 and references therein). The Iapetus Ocean started to close in the Cambrian following development of a southeastward dipping (ocean-facing) subduction zone near Laurentia which formed the Grampian-Taconic arc (Fig 1a). During the early-middle Ordovician (ca. 490–465 Ma), the Laurentian margin was partially subducted under the arc, resulting in ophiolite obduction, HP metamorphism and regional deformation and metamorphism of footwall Dalradian and Moine metasedimentary successions of the NHT and GT – the Grampian orogenic event (Lambert & McKerrow 1976; Dewey & Shackleton 1984; Friedrich et al. 1999; Friend et al. 2000; Oliver et al. 2000; Chew & Strachan, 2014; Johnson et al. 2017). This was followed by Late Ordovician metamorphism at ca. 455–445 Ma (Bird et al. 2013), and Silurian metamorphism and deformation at ca. 444–415 Ma, both confined to the Northern Highland Terrane (NHT) (Fig. 2a). The sinistrally oblique Laurentia-Avalonia collision has been considered as a 'soft' collision (Soper & Woodcock 1990), without causing significant crustal thickening. Palaeomagnetic and faunal data indicate that the northern Iapetus Ocean did not close until ca. 420 Ma (Soper & Woodcock 1990), thus most of the orogenesis pre-dated final continental collision.

There are, however, significant gaps in our current understanding of Caledonian tectonics. The thermal evolution of GT Dalradian rocks is well understood as they were not significantly overprinted after the Grampian orogenic event. In contrast, the thermal evolution of NHT Moine rocks is more complex. Neoproterozoic regional metamorphic assemblages were overprinted during the Caledonian orogeny *sensu lato* (Law et al. 2024; Strachan et al. 2024 and references therein). The pressure-temperature (PT) conditions and tectonic driver(s) of the ca. 455–445 Ma event, and whether this is distinct from the Grampian and Scandian events, are also uncertain (Bird et al. 2013; Searle 2021; Walker et al. 2021; Law et al. 2024). Here we show that ca. 455–445 Ma mineral assemblages on the Ross of Mull within the Scottish Caledonides are associated with regional HP conditions. We interpret this as the early stage of a protracted Late Ordovician-Silurian accretionary mountain building event which predated closure of the Iapetus Ocean and terminal continental collision.

Regional setting

The Ross of Mull is located in the NHT and exposes a synformal inlier of Moine rocks and associated metabasic intrusions (Figs 2 & 3). Across the NHT, the Moine rocks are stacked as three nappes, collectively defining an inverted Caledonian metamorphic gradient resulting from syn- to post-metamorphic thrusting (Fig. 2a; Mazza et al., 2018). These nappes include:

(1) The Naver Nappe which underwent HP metamorphism during the Grampian orogenic event, as indicated by garnet-clinopyroxene bearing assemblages that equilibrated at *P*–*T* conditions of 1.0–1.2 GPa and 650–700°C (Friend et al. 2000). A sillimanite-grade event followed at *P*–*T* conditions of ca. 0.8–0.9 GPa and 600°C with decompression and heating to 0.6–0.7 GPa and 700 °C dated at ca. 444–415 Ma by U–Pb monazite and xenotime (Ashley et al. 2015; Mako et al. 2019). Sm–Nd and Lu–Hf Caledonian garnet dates indicate garnet growth between ca. 454–446 Ma, although the metamorphic conditions are unknown.

(2) The Sgurr Beag Nappe with kyanite and sillimanite-bearing assemblages that record *P*–*T* conditions of 0.7–0.9 GPa and 650–700°C, with U–Pb monazite and titanite dates spanning ca. 473–464 Ma (Cutts et al. 2010; Mako et al. 2019) and Sm–Nd and Lu–Hf garnet dates spanning ca. 475–463 Ma (Bird et al. 2013).

(3) The Moine Nappe which is associated with a decrease in *P*–*T* conditions westward, and down-structural section, from 0.82 GPa and 680 °C in the east to 0.42 GPa and 550 °C in the west of the hanging-wall of the Moine Thrust (Ashley et al. 2015; Mazza et al. 2018; Mako et al. 2019). U–Pb zircon ages from syn-thrusting plutons as well as monazite and xenotime ages are consistent with Scandian nappe stacking and metamorphism between ca. 444–415 Ma (Mako et al. 2019; Strachan et al. 2020). Lu–Hf and Sm–Nd garnet geochronology suggest garnet growth mainly between ca. 455–445 Ma (Bird et al. 2013).

Widespread upright 'D3' folding affected both the Sgurr Beag and Moine nappes after they had been juxtaposed to form the Northern Highland Steep Belt. D3 folding is bracketed by the 448.7 ± 2.9 Ma intrusion age of the deformed Glen Dessary syenite (U–Pb zircon; Goodenough et al. 2011) and the 431.6 ± 1.3 Ma intrusion age of the cross-cutting and undeformed Cluanie Pluton (U–Pb zircon; Milne et al. 2023) (Fig. 2). Formation of the Northern Highland Steep Belt thus plausibly overlapped the ca. 455–445 Ma metamorphic event recorded by Bird et al. (2013) in the NHT and Walker et al. (2021) on Shetland.

On the Ross of Mull, the Moine rocks are exposed as a 6-km section to the east of the Ross of Mull granite pluton (Fig. 3) (dated by U-Pb zircon at 418 ± 5 Ma; Oliver et al. 2000). Kyanite bearing mineral assemblages are regionally observed and overprinted by andalusite, sillimanite and K-feldspar, associated with the metamorphic aureole of the Ross of Mull pluton (Wheeler et al. 2004). On the western side of the Ross of Mull pluton, on the Isle of Iona, cordierite occurs within the Iona group sediments, interpreted to be part of the Neoproterozoic Torridon Group in the Caledonian foreland. This suggests that the Ross of Mull pluton cuts across the projection of the Moine Thrust and the cryptic Sound of Iona (SIF, Figure 3) normal fault. It is possible that this structure influenced the intrusion of the Ross of Mull pluton, as inferred by top-to-east normal sense shear fabrics observed in the Iona Group metasediments (Zaniewski et al. 2006).

To the east of the Ross of Mull pluton, the Moine rocks are folded into a synform (the Assapol synform). The structurally lowest Moine rocks correlate with the Morar Group and the structurally highest with the Glenfinnan Group (Holdsworth et al. 1987), and are separated by an intervening shear zone, although it remains uncertain whether this is the Sgurr Beag Thrust (Holdsworth et al. 1987 vs. Krabbendam et al. 2022). In the Glenfinnan Group (the structurally highest rocks), meta-sandstones are intercalated with metabasic sheets (now garnet amphibolites) and metapelitic schists (with garnet, biotite, muscovite and locally kyanite). Published thermobarometry is restricted to the latter with *P*–*T* conditions estimated at 0.8 GPa at a temperature of 600–650°C (Wheeler et al. 2004). However, the timing of kyanite grade metamorphism has hitherto been unknown. Bird et al. (2013) reported a 448.7 ± 5 Ma Lu–Hf garnet age from a garnet amphibolite at Ardalanish Bay (Fig. 3), similar to ca. 455–445 Ma Lu–Hf garnet dates recorded regionally across the Moine and Naver nappes on mainland Scotland. However, it is unclear what *P*–*T* conditions these garnet dates relate to. The rocks on the Ross of Mull therefore represent an opportunity to determine the *P*–*T* conditions of this hitherto poorly understood Late Ordovician metamorphism in the Scottish Caledonides as they are likely located at an intermediate structural level within thrust sheets of the NHT (Figs. 2A, 3A).

Field Relationships and Petrography

Two samples of garnet amphibolite (19TL20, 19TL21) were collected from ~2–15 m wide NNE-SSW trending mafic bodies at Ardalanish Bay, approximately 1 km east of the Ross of Mull Granite (Fig. 4). A metapelite (WMAR007) was also collected from ~700 m to the east of the Ross of Mull pluton. Outcrop relations and sample photomicrographs are presented in Figures 4 and 5, respectively. The amphibolites are characterized by garnet porphyroblasts with rotational inclusion trails (S_1), that are discordant to the amphibole-bearing matrix which exhibits a continuous internal foliation (S_2), (Figures 4 and 5). This foliation is parallel with the foliation of the metasedimentary host rock that is deformed into westward verging minor folds (Fig. 5), therefore indicating the same metamorphic and deformation history. Millimetre to centimetre sized segregations of leucosome are locally aligned with S_2 in the amphibolite (Fig. 5) and have trondhjemitic (plagioclase-quartz) compositions, indicating that conditions locally surpassed the water saturated solidus (Weinberg et al., 2015; Palin et al., 2016). Metapelites contain garnet, biotite, muscovite, rutile and locally K-feldspar and kyanite and have similarly trondhjemitic leucosome segregations that are ptygmatically folded and also display a westward fold vergence direction. A penetrative spaced foliation (S_2) is axial planar to these folds and often defined by alignment of muscovite (Figs 5 and 6). These observations suggest that westward directed shearing occurred during or shortly following anatexis.

Within the metabasic bodies, a bimodal distribution of garnet sizes occurs in discrete 30 cm to metre sized domains that are oriented parallel with intrusion margins (Fig. 4B). Sample 19TL20 has abundant small garnets and 19TL21 contains fewer but larger cm-sized garnets, although both samples have similar proportions of garnet (15%), ilmenite (7%), quartz (10%), rutile (0.5%) and titanite (0.7%) with leucocratic plagioclase (9%). Domains with smaller garnets (19TL20) contain no biotite or epidote and more amphibole (56%) whereas domains with larger garnets (19TL21) have greater abundances of hydrous phases (13% biotite and 3% epidote) and although less amphibole (42%) and are associated or in contact with trondjhemitic leucosomes (Fig. 5).

In contrast, metapelite sample WMAR007 preserves compositional layering (S_0) that is characterized by mica-rich domains with muscovite and biotite up to several cm across. Fine grained quartzo-felspathic domains up to 1 cm wide containing plagioclase quartz, garnet, and K-feldspar that define S_1. S_1 is subsequently folded on the cm-metre scale forming crenulations, with a penetrative spaced foliation (S_2) aligned axial planar to the folds. Garnets often show atoll-like textures (Fig. 5), with the core replaced by biotite, plagioclase and muscovite, and the outer rims resorbed by retrograde biotite. However, in some garnets (e.g., garnet 1), the core is partially preserved. Rutile, ilmenite and titanite also occur as secondary phases throughout the matrix, consistent with a HP assemblage variably overprinted by retrogression. Although kyanite was seen in micaceous layers at outcrop, the thin section used for thermobarometry from sample WMAR007 does not contain kyanite.

Mineral Chemistry

The compositions of phases in samples 19TL20, 19TL21 and WMAR007 were derived from a CAMECA SX5-FE (field emission) electron microprobe at the Department of Earth Sciences, University of Oxford. Operating conditions involved an accelerating voltage of 15.0 keV corresponding to a current of 20 nA, a range of primary and secondary standards were used including andradite (Fe, Mg, Ca), TiO_2 (Ti), Mn metal (Mn), labradorite (Na, Al, Si) and sanidine (K) for major elements and synthetic standards for (from the University of Edinburgh) for the rare earth elements (REE's). Garnet line profiles were collected using a 10-μm step size across all garnets. Mineral abbreviations follow the guidelines of Whitney and Evans (2010). Anhydrous phase compositions were calculated to standard numbers of oxygen per formula unit (Deer et al., 1992), micas were recalculated to 11 oxygens, and chlorite to 28 oxygens. Where present, H_2O content was assumed to occur in stoichiometric amounts. The proportion XFe^{3+} (Fe^{3+}/Fe_{total}) was calculated using AX (Holland, 2009) and amphibole exchange vectors were calculated using the method of Droop, (1987), the complete electron probe microanalyses are presented in Supplementary Table S1.

In garnet amphibolite samples 19TL20 and 19TL21, chemical traverses across garnets show overlapping, flat and homogenised profiles [X_{Alm}(0.56-0.63) X_{Prp}(0.12-0.14), X_{Grs}(0.24-0.27) and X_{Spss}(0.02-0.04)] (Fig. 5). These flat profiles are observed irrespective of garnet size. Matrix amphiboles across these two samples have similar Tschermakitic-Ferro-tschermakitic compositions (Supplementary Material). The similarity in garnet and amphibole chemistry and modal abundances between the two samples is consistent with almost identical bulk rock chemical compositions derived from X-ray fluorescence. However, subtle differences do occur between samples. Domains containing cm-sized, fewer garnets (sample 19TL21), have greater abundances of hydrous phases (biotite and epidote) and are closely associated or in contact with trondhjemitic leucosomes (Fig. 4). This suggests that domains with larger garnets were more hydrated and that garnet growth in the amphibolites was facilitated by the presence of fluid or melt. This is also apparent from the increased stability of garnet with increasing Molar H_2O at a given pressure and temperature in sample 19TL20 (see below and in Fig. 7). Whereas in sample WMAR007 garnets show an increase in spessartine (Mn) content from core to outer rim, indicative of garnet resorption by biotite and retrograde net transfer reactions (Kohn and Spear, 2000). In contrast, pyrope, grossular and almandine decrease from the garnet cores to outer rims [X_{Alm}(0.72-0.60) X_{Prp}(0.08-0.06), X_{Grs}(0.20-0.10) and X_{Spss}(0.02-0.10)] (Fig. 5). These features suggest peak conditions are most likely to be preserved in the garnet cores or interior, whereas the garnet rims likely constrain retrogression during exhumation.

Thermobarometry

Thermobarometric calculations were performed using the following methods, Amphibole-plagioclase thermometry (Holland and Blundy, 1994) was used for the amphibolites and Ti-in-biotite thermometry (Henry et al., 2005) was used for biotite and graphite bearing samples (19TL21 and WMAR007). Garnet-biotite thermometry (Bhattacharya et al., 1992; Holdaway, 2000) and garnet-aluminosilicate-plagioclase and garnet-plagioclase-muscovite-biotite barometry (Spear, 1993) was used for metapelite sample WMAR007. THERMOCALC Average PT mode and dataset 62 (Holland and Powell, 2011) was used for all samples. The full results are presented in Figs. 6-8 and Table 1.

Amphibole-plagioclase thermometry (Holland and Blundy, 1994), predicts a mean temperature for sample 19TL21 of 671 ± 15°C using the Edenite-Tremolite thermometer and 688 ± 21°C for the Edenite-Richterite thermometer using the average matrix plagioclase anorthite composition (An = 0.28). In contrast, sample 19TL20 records a mean temperature of 665 ± 15°C for the Edenite-Tremolite thermometer and 717 ± 34°C for the Edenite-Richterite thermometer (Supplementary Material). Ti-in-biotite thermometry (Henry et al. 2005) predicts peak temperatures of 748 ± 12°C for sample WMAR007, and 723 ± 12°C for sample 19TL21, and with most biotite analyses clustering around 660–670°C (Supplementary Material), similar to amphibole-plagioclase thermometry. These results suggest that most biotite is retrograde, and peak metamorphic temperatures in all samples likely exceeded 720°C.

For metapelite sample WMAR007, garnet-biotite thermometry combined with garnet-aluminosilicate-plagioclase (GASP) and garnet-plagioclase-muscovite-biotite (GPMB_Mg) barometry suggest that the garnet core (Grt 1) attained 638°C ± 30°C and 1.28 GPa (GPMB_Mg), 1.04 GPa (GPMB_Fe) and 1.07 GPa (GASP) ± 0.12 GPa respectively. However, caution must be taken with the GASP result as although kyanite was seen in outcrop, the thin section sample did not contain kyanite. The GMB result is considered robust, although calculated Grt-Bt temperatures likely represent a minimum due to retrograde net transfer reactions (Kohn and Spear, 2000). In contrast, garnet rims in contact with biotite record retrograde conditions (Grt 4) of 496 ± 30°C and 0.53 GPa (GASP), 0.67 GPa (GPMB_Mg) and 0.51 GPa (GPMB_Fe) ± 0.12 GPa respectively. These results suggest cooling of the sample through the kyanite stability field (Fig. 8) and is consistent with the observation of andalusite pseudomorphing kyanite and the lack of regional sillimanite (Wheeler et al. 2004).

Calculations using THERMOCALC Average PT mode, based on garnet core compositions and average matrix compositions suggest that the assemblage Grt-Amp-Fsp-Rt-Ilm-Qz-Sph-H_2O in sample 19TL20 equilibrated at 1.06 GPa ± 0.13 GPa and 755 ± 96°C whereas Grt-Amp-Bt-Pl-Rt-Ilm-Ep-Qz-Sph-H_2O in sample 19TL21 attained 1.02 GPa ± 0.11 GPa and 777 ± 54°C (Fig. 8). Calculations on metapelite sample WMAR007 using garnet cores and the observed assemblage Grt-Ms-Bt-Kfs-Pl-Qz-Rt-Ilm-H_2O suggest that it attained 1.06 ± 0.14 GPa and 750 ± 41°C (Fig. 8).

Petrological Modelling

Petrological modelling was performed in Theriak-Domino (de Capatani, 2010) using Dataset 62 (Holland and Powell, 2011) using the bulk compositions determined by X-ray fluorescence (XRF) (Table S2). An XFe^{3+} = 0.3 was used in modelling amphibolites based on an estimated bulk rock composition from using amphibole compositions as a proxy. Temperature-M(O) phase diagram calculations for 19TL20 at a pressure of 1.0 GPa also best reproduce the observed assemblage (Grt-Amp-Pl-Qz-Rt-Ilm-Liq±Rt) when XFe^{3+} ~ 0.1–0.35 which is within error of average Fe^{3+} values for metabasites = 0.26 ± 0.12 (Forshaw et al. 2024) (Fig. 7). For metapelite sample WMAR007, an XFe^{3+} = 0.3 was also used, which is within error of the global median Fe^{3+} = 0.23 for metapelites (Forshaw and Pattison, 2023). Bulk rock H_2O contents used in modelling for amphibolite samples 19TL20 and 19TL21 was 4.5%mol, which was determined by minimally saturating the solidus at a pressure of 0.75 GPa (Fig. 6A, B), with free H_2O as a volatile phase removed from the assemblage within 10°C of the solidus. In contrast, in metapelite sample WMAR007 the loss on ignition (LOI) determined from XRF was used for the H_2O as primary muscovite remained stable at peak conditions and therefore the measured bulk rock water content likely represents the water content within the rock at peak conditions. For amphibolite samples 19TL20 and 198TL21, the activity-composition models for amphibole, clinopyroxene, orthopyroxene, biotite, chlorite, garnet and melt (Green et al., 2016); ternary feldspar (Holland et al., 2022); epidote (Holland et al., 2011); white mica (White et al., 2014) and ilmenite (White et al., 2000) were used. Because Mn is negligible in both amphibolites, and Mn bearing activity models for amphibole are not available, calculations were performed in the 10-component system Na_2O-CaO-K_2O-FeO-MgO-Al_2O_3-SiO_2-H_2O-TiO_2 (NCKFMASHTO). In contrast, for metapelite sample WMAR007, Mn was included in the calculations, and the pelite models for garnet, biotite, white mica, staurolite, chlorite, melt, orthopyroxene and cordierite were used (White et al. 2014). The phase diagrams are presented in Figs. 6-7.

Phase diagram results show that garnet-bearing fields in the amphibolites are confined to pressures exceeding 0.9 GPa (Fig. 6A-B). This provides a minimum pressure constraint for garnet growth, and therefore a direct link between the ca. 448 Ma Lu–Hf date and high-pressure metamorphic conditions (Figs. 6-7). A phase diagram for sample 19TL20 (Fig. 6A) predicts clinopyroxene stable across the pseudosection, which is inconsistent with the observed assemblage. This is a well-known issue with the augite activity-composition model of Green et al. (2016), but it does not affect the stability of other major phases (e.g., Forshaw et al., 2018). Furthermore, the predicted Cpx is negligible (<2% volume), and therefore ignoring Cpx, the peak assemblage Grt-Amp-Pl-Qz-Rt-Ilm-Liq for sample 19TL20 is reproduced between 750–900°C and 1.05–1.40 GPa. Intersection of garnet isopleths X_{Prp}(0.13), X_{Grs}(0.26) and the observed (15%) garnet volume place even tighter *P*–*T* constraints of 1.05–1.30 GPa and 790–810°C. (Fig. 6C, E).

In contrast, the phase diagram of sample 19TL21 (Fig. 6B) does not predict Cpx until much higher temperatures and the peak assemblage Grt-Amp-Pl-Bt-Rt-Ilm-Qz-Liq is reproduced at 1.08–1.3 GPa and 750–810°C. Intersection of the observed garnet isopleths X_{Prp}(0.13), X_{Grs}(0.26) and the observed (15%) garnet volume place even tighter *P–T* constraints of 1.08–1.30 GPa and 760–780°C (Fig. 6D, F). These calculated *P–T* constraints overlap within uncertainty, which is encouraging given the samples were taken less than 1 metre apart.

A calculated phase diagram for metapelite sample WMAR007 (Fig. 7C) using an XFe^{3+} = 0.3 predicts the observed assemblage Grt-Ms-Bt-Pl-Kfs-Ilm-Rt-Qz-Liq in a small stability field at 1.30-1.32 GPa and 750-760°C. Garnet core isopleths intersections X_{Prp}(0.08), X_{Grs}(0.20) constrain conditions ~1.2–1.3 GPa and 720–750°C in the Kfs absent Grt-Ms-Bt-Pl-Ilm-Rt-Qz-Liq field (Fig. 7D). This field is however directly adjacent to, and within ~10°C of the predicted appearance of K-feldspar, which is within uncertainty of the model results (Palin et al. 2016) and therefore is in good agreement with observations. Due to the elevated pressures predicted, these results suggest that peak metamorphic conditions did not surpass muscovite breakdown (which has a positive reaction *P–T* slope). This is consistent with the presence of primary muscovite in WMAR007, and evidence for trondjemitic leucosomes that are heterogeneously distributed across Ardalanish Bay. Both these observations suggest that anatexis occurred by the local addition of water rather than incongruent melting of muscovite. However, we acknowledge that closer to the Ross of Mull Pluton, muscovite is absent, and fibrolitic sillimanite and K-feldspar occur in the groundmass, inferred to be a result of muscovite breakdown at lower pressure (~0.3 GPa) after the HP kyanite grade event (Wheeler et al. 2004) (Fig. 7).

Discussion

Integration of the new *P*–*T* constraints with published Lu–Hf garnet geochronology from the same amphibolite suite (Bird et al. 2013) reveals that the 448.7 ± 5 Ma garnet date constrains peak HP metamorphic conditions to ca. 1.0–1.2 GPa and 700–780°C (Fig. 8). This is because garnet bearing fields in the amphibolites are constrained to pressures exceeding 0.9 GPa, whereas in metapelites garnet growth can occur at lower pressure due to more Mn in the bulk composition. A near identical Lu–Hf garnet age of 447.3 ± 1.7 Ma was obtained by Bird et al. (2013) from a similar metabasic intrusion in the Moine Nappe on the north coast of Scotland (Fig. 2A). Walker et al. (2021) also presented Lu–Hf garnet ages from similar garnet amphibolites on Shetland of 453.6 ± 5.1 Ma and 449.2 ± 2.3 Ma, and 452.0 ± 1.4 Ma from a kyanite bearing gneiss. Together, these data suggest that similar HP conditions likely extended along the western NHT and Shetland between ca. 455–445 Ma, and requires a (now removed) ~40 km thick overburden.

At this time, rocks in the overlying thrust sheets in the eastern NHT (Sgurr Beag and Vaver Nappes) and the GT show no record of the HP metamorphism and were presumably experiencing exhumation and cooling (Mako et al. 2019; Law et al. 2024), following earlier burial, underplating and Ordovician metamorphism due to the Grampian arc-continent collision at ca. 490–480 Ma (Friend et al. 2000; Kutts et al. 2011). However, we see no evidence on the Ross of Mull for a regional lower-pressure sillimanite-grade metamorphism between ca. 444–415 Ma that is recorded in the underlying northern Moine Nappe (Mako et al., 2019; Mazza et al., 2018; Fig. 2). The Ross of Mull kyanite-bearing rocks therefore likely occur at structurally intermediate levels of the orogenic wedge and were not overprinted by later high-temperature regional metamorphism.

Within the contact aureole of the Ross of Mull Granite (Fig. 3B), cordierite, sillimanite, and andalusite overprint earlier kyanite-bearing assemblages at 0.3 GPa and 500–750°C (Wheeler et al., 2004). This requires substantial exhumation of rock associated with decompression from ca. 1.1–0.3 GPa between ca. 449–418 Ma. This necessitates the removal of ~30 km of crust at a rate of ~1 km/ Myr. No regionally significant extensional detachments have been identified (Law et al. 2024), and so exhumation and cooling are here related to erosion driven by contemporaneous, and continued convergence and underplating of the Laurentian foreland, ultimately resulting in the development of the Moine Thrust Zone at ca. 430 Ma.

Because the ca. 455–445 Ma HP episode is confined to the NHT and was followed by metamorphic ages spanning ca. 444–415 Ma (Mako et al. 2019), it has been suggested that it represents a single, protracted Late Ordovician-Silurian orogenic event (Law et al. 2024) that commenced prior to closure of the Iapetus Ocean at ca. 420 Ma. The HP metamorphic garnet ages presented by Bird et al. (2013) and Walker et al. (2021) also shortly follow the 'Grampian' metamorphic ages by only ~4 Myrs. Assuming realistic rates of convergence and dip of thrust faults resulting in the burial of rock to depths of 40 km required by our metamorphic pressures of 1.2 GPa, this raises the possibility that the Caledonian Orogeny in Scotland formed semi-continuously and diachronously over a protracted ca. 50 Myr period.

However, the new data could be consistent with several competing tectonic models that might account for such a protracted period of Caledonian orogenesis prior to continental collision. At least three models need to be considered (Fig. 9): (1) a post-Grampian flip to NW-dipping subduction was followed by Late Ordovician to Silurian orogenesis in the NHT due to accretion of outboard terranes (Bird et al. 2013) and/or segments of southern Baltica (Law et al. 2024), followed by ca. 700 km of late Silurian-Devonian strike-slip displacement along the Great Glen Fault (GGF) to juxtapose the NHT and GT in their present relative positions (Dewey & Strachan 2003) (Fig. 9A). This model may explain the consistent timing of ca. 455–445 Ma HP metamorphism confined to the NHT as a discrete event, however, such cryptic accreted micro-continental terranes are not exposed, and the timing of the Baltica collision is constrained to ca. 430–420 Ma after the ca. 455–445 Ma period of crustal thickening and HP metamorphism; (2) GGF displacements are minimal and continuous SE-directed underthrusting of Laurentia beneath the Midland Valley arc caused the locus of crustal thickening and metamorphism to migrate northwestwards from the GT across the NHT over ca. 50 Myrs (Searle, 2021) (Fig 9B). This model is consistent with the diachroneity of deformation and metamorphism migrating towards the Laurentian foreland but cannot explain the eventual closure of the Iapetus without establishing another subduction zone to the south of the Midland Valley Terrane. As such, Model 2 promotes an accretionary system; alternatively (3) subduction flip during/after the Grampian event was followed by NW-dipping flat-slab subduction that drove the locus of contractional deformation, magmatism and metamorphism inboard (NW) from the trench (Bird et al. 2013; Dewey et al. 2015) (Fig. 9C). In this model, there is no need for a cryptic micro-continent as in Model 1, yet it can explain closure of the Iapetus to the south of the Midland Valley. Notably, we compare this latter style of convergence with the North America Cordillera, where major crustal thickening and high-grade metamorphism during the Laramide Orogeny was related to flat-slab subduction during the Late Cretaceous to Paleocene due to increased tractions along the plate interface and end-load at the trench (Yonkee & Weil, 2015 and references therein; Lamont et al. 2024). This could account for the ca. 455–445 Ma HP regional metamorphism prior to terminal continental collision. In addition, later rollback of the low-angle slab would also increase asthenospheric heat-flow, and cause melting of the sub-continental lithosphere that was previously hydrated during the earlier phase of flat-slab subduction, ultimately forming the 'Newer Granites' at ca. 430–400 Ma (Milne et al. 2023).

Irrespective of the preferred tectonic model, our data suggest that the Caledonian Orogen in Scotland was an accretionary mountain belt with the climax of orogenesis occurring prior to terminal continental collision of Laurentia, Avalonia and Baltica. This is very different from the East Greenland (Laurentia) and Norway (Baltica) collision (Fig. 1C) along strike, where HP metamorphism was associated with the final Iapetus closure and extended into the Devonian (Weller et al. 2021).

Conclusions

We conclude that Late Ordovician HP metamorphism in the Scottish Caledonides shortly followed the Grampian arc-continent collision but *predated* closure of the Iapetus Ocean. The newly recognized HP metamorphism, reaching conditions of 1.0–1.2 GPa and 700–780 °C at ca. 455–445 Ma likely reflects a period of accretionary orogenesis that was continuous with terminal continental collision at ca. 430–425 Ma.

These contrasting styles and timing of crustal thickening and regional HP metamorphism along the Iapetus Suture of the Caledonian Orogen emphasize that protracted periods of mountain building throughout earth's history need not always require terminal continental collision (Dewey 1982, Cawood et al. 2011).

Acknowledgements

This research benefitted from discussions with Richard White, Tony Prave, Maarten Krabbendam, Sebastian Fischer and Jacob Forshaw. We would like to extend thanks to Jon Wade for kindly providing EPMA time, and Jon Wells for preparing thin sections. We would also like to thank Tim Johnson and Rick Law for providing constructive and helpful reviews of an earlier version of the manuscript.

Figures

Figure 1. Plate tectonic reconstruction for the Iapetus Ocean and Caledonian Orogeny based on Chew and Strachan, (2014).

Figure 2. A) Terrane map of the Caledonian Orogeny in Scotland B) Simplified geological map of Scotland and *P*–*T*–t compilation, C) Summary of geochronological data from the NHT and GT.

Figure 3: Schematic cross section through the Northern Highland Terrane, showing the likely structural level for the Ross of Mull in relation to the larger scale structures.

B-D) Simplified geological map and cross sections of the Ross of Mull showing sample locations, structures and key cross-cutting relationships.

Figure 4) Field photographs showing kyanite grade metamorphic assemblages and partial melting at Ardalanish Bay. A) Outcrop photographs of kyanite grade assemblages and partial melting metapelites with pytmatically folded trondjhemitic leucosomes containing peritectic garnet. B) Garnet amphibolite with larger garnets concentrated along leucosomes. C) Retrogressed kyanite schist with kyanite pseudomorphed by andalusite. D) Garnet amphibolite with peritectic garnet in leucosome with plagioclase and quartz. E) metapelitic migmatite with leucosomes aligned parallel to S_1 which are folded, and affected by boudinage along S_2 (sub-horizontal east-west trending foliation) subparallel to the fold axes. F) Mesoscale trondhjemitic leucogranite sill derived from the amphibolite. G) Outcrop of sample WMAR007 with micaceous and quartz-felspathic banding, likely representing compositional layering (S_0-S_1). H) Outcrop photograph of the amphibolite (metabasic intrusion) on Ardalanish Bay, showing the locations of 19TL20 and 19TL21 as well as the continuous S_2 foliation of the amphibolite with the surrounding metasediments.

Figure 5. Photomicrographs of samples used in the study showing locations of garnet line profiles. A-B) garnet amphibolites samples 19TL20 and 19TL21 showing continuous matrix foliation which largely postdates garnet growth, note discordance between S_1 trapped as inclusions in garnet and the external matrix foliation S_2. C-D) Photomicrograph of sample WMAR007showing garnet breakdown textures to biotite, enclaved in primary muscovite. E-F) characteristic chemical line profiles across garnet used for thermobarometry.

Figure 6. Equilibrium phase diagrams of samples 19TL20 and 19TL21, A) 19TL20 predicted phase fields showing the peak assemblage in red text (excluding Cpx), B) Equilibrium phase diagrams of sample 19TL21 showing the peak assemblage field in red text, C) 19TL20 pyrope and grossular garnet isopleths, the green polygon represents the observed garnet composition X_{Prp}(0.13) and X_{Grs} (0.27), D) 19TL21 pyrope and grossular garnet isopleths, the green polygon represents the observed garnet composition X_{Prp}(0.12) and X_{Grs}(0.27). E) Predicted garnet modal proportions (vol%) for amphibolite samples 19TL20 and F) 19TL21, showing good agreement between observed ~15% volume garnet and garnet isopleth intersections in both samples.

Figure 7. A) Binary equilibrium phase diagram of sample 19TL20 at a pressure = 1.0 GPa, A) XFe^{3+} varying from 0-0.6 equating to varying molar O from 0.006% to 3.690%, B) Molar (H_2O) varying from 0.05-20%. Calculated assemblage fields most closely match observations (red text) when XFe^{3+} ~ 0.3 and M(H_2O) = 4-15%, although rutile bearing fields require higher pressures and suggest metamorphic conditions occurred at 1.1 GPa. C) Equilibrium phase diagrams of sample WMAR007, predicted assemblage fields and the peak assemblage in red text, D) pyrope and grossular garnet composition isopleths, the green polygon represents the observed garnet composition X_{Prp}(0.075) and X_{Grs}(0.20).

Figure 8. Summary *P–T–t* path for the Ross of Mull. *P–T–t* data for the Naver Nappe (Friend et al. 2000), Sgurr Beag Nappe (Cutts et al. 2010) and Moine Nappe (Ashley et al. 2015; Mazza et al. 2019) are shown for comparison.

Figure 9. Competing tectonic models for the Scottish Caledonides; A) Discrete orogenic events model of Bird et al. (2013) related to i) collision of the Midland Valley Arc resulting in the 'Grampian Orogeny', ii) collision of a cryptic microcontinent resulting in the 'Grampian II Orogeny', and iii) collision of Baltica resulting in the 'Scandian Orogeny' before ca. 700km sinstral motion on the Great Glen Fault. B) Continuous SW-directed underthrusting of Laurentia model of Searle, (2021), resulting in diachronous metamorphism and deformation that migrated towards the NW with time with minimal off-set on the Great Glen Fault. C) Flat-slab subduction model after a post-Grampian 'subduction flip', resulting in diachronous deformation and metamorphism, without necessarily requiring large offsets on the Great-Glen Fault. Subsequent slab-rollback after ca. 430 Ma would cause melting of the previously hydrated lithospheric mantle that was previously hydrated during flat-slab subduction, resulting in the 'Newer Granites'.

References

Bhattacharya, L., Mohanty, L., Maji, A., Sen, S.K., and Raith, M., (1992). Non-ideal mixing in the phlogopite-annite binary: Constraints from experimental data on Mg-Fe partitioning and a reformulation of the biotite-garnet geothermometer: *Contributions to Mineralogy and Petrology*, 111, 87–93, https://doi.org/10.1007/BF00296580.

Bird, A. F., Thirlwall, M. F., Strachan, R. A., & Manning, C. J. (2013). Lu–Hf and Sm–Nd dating of metamorphic garnet: evidence for multiple accretion events during the Caledonian orogeny in Scotland. *Journal of the Geological Society*, 170(2), 301-317.

Cawood, P. A., Leitch, E. C., Merle, R. E., & Nemchin, A. A. (2011). Orogenesis without collision: Stabilizing the Terra Australis accretionary orogen, eastern Australia. *Bulletin*, *123*(11-12), 2240-2255.

Chew, D. M., and Strachan, R. A. (2014). The Laurentian Caledonides of Scotland and Ireland. In New Perspectives on the Caledonides of Scandinavia and Related Areas (eds F Corfu, D Gasser and DM Chew), 45–91. *Geological Society of London*, Special Publication, 390.

Cutts, K.A., Kinny, P.D., Strachan, R.A., Hand, M., Kelsey, D.E., Emery, M., Friend, C.R.L. and Leslie, A.G. (2010). Three metamorphic events recorded in a single garnet: Integrated phase modelling, in situ LA-ICPMS and SIMS geochronology from the Moine Supergroup, NW Scotland. *Journal of Metamorphic Geology*, 28(3) 249-267.

de Capitani, C., and Petrakakis, K. (2010). The computation of equilibrium assemblage diagrams with Theriak/Domino software. *American Mineralogist*, 95,1006-1016.

Droop G. T. R. (1987). A general equation for estimating Fe3+ concentrations in ferromagnesian silicates and oxides from microprobe analyses, using stoichiometric criteria. *Mineralogical Magazine*. 51(361), 431-435. doi:10.1180/minmag.1987.051.361.10

Dewey, J. F., (1982). Plate tectonics and the evolution of the British Isles: Thirty-fifth William Smith Lecture, Journal of the Geological Society, 139, 371 – 412 https://doi.org/10.1144/gsjgs.139.4.0371

Dewey, J. F., and Shackleton, R. J. (1984). A model for the evolution of the Grampian tract in the early Caledonides and Appalachians. *Nature*, 148, 137–80.

Dewey, J. F., & Strachan, R. A. (2003). Changing Silurian–Devonian relative plate motion in the Caledonides: sinistral transpression to sinistral transtension. *Journal of the Geological Society*, *160*(2), 219-229.

Dewey, J. F., Dalziel, I. W. D., Reavy, R. J. and Strachan, R. A. (2015). The Neoproterozoic to Mid-Devonian evolution of Scotland: a review and unresolved issues. *Scottish Journal of Geology*, 51, 5–30.

Dunk, M., Strachan, R. A., Cutts, K. A., Lasalle, S., Storey, C. D., Burns, I. M., ... & Pereira, I. (2019). Evidence for a late Cambrian juvenile arc and a buried suture within the Laurentian Caledonides of Scotland: Comparisons with hyperextended Iapetan margins in the Appalachian Mountains (North America) and Norway. *Geology*, 47(8), 734-738.

Forshaw, J. B., & Pattison, D. R. (2023). Major-element geochemistry of pelites. *Geology*, *51*(1), 39-43.

Forshaw, J. B., Waters, D. J., Pattison, D. R., Palin, R. M., & Gopon, P. (2019). A comparison of observed and thermodynamically predicted phase equilibria and mineral compositions in mafic granulites. *Journal of Metamorphic Geology*, *37*(2), 153-179.

Forshaw, J. B., Dominguez, H., Markmann, T. A., Tamblyn, R., Hermann, J., Riel, N., & Lanari, P. (2024). Major-element geochemistry and Fe3+/ΣFe of metabasites. *Journal of Petrology*, *65*(12), egae120.

.

Friedrich, A. M., Bowring, S. A., Martin, M. W., & Hodges, K. V. (1999). Short-lived continental magmatic arc at Connemara, western Irish Caledonides: Implications for the age of the Grampian orogeny. *Geology*, *27*(1), 27-30.

Friend, C. R. L., Jones, K. A., & Burns, I. M. (2000). New high-pressure granulite event in the Moine Supergroup, northern Scotland: Implications for Taconic (early Caledonian) crustal evolution. *Geology*, 28(6), 543-546.

Goodenough, K. M., Millar, I., Strachan, R. A., Krabbendam, M., & Evans, J. A. (2011). Timing of regional deformation and development of the Moine Thrust Zone in the Scottish Caledonides: constraints from the U–Pb geochronology of alkaline intrusions. *Journal of the Geological Society*, *168*(1), 99-114.

Green, E. C. R., White, R. W., Diener, J. F. A., Powell, R., Holland, T. J. B. & Palin, R. M., (2016). Activity-composition relations for the calculation of partial melting equilibria in metabasic rocks. *Journal of Metamorphic Geology*, 34, 845-869. doi:10.1111/jmg.12211

Henry, D. J., Guidotti, C. V., & Thomson, J. A. (2005). The Ti-saturation surface for low-to-medium pressure metapelitic biotites: Implications for geothermometry and Ti-substitution mechanisms. *American mineralogist*, 90(2-3), 316-328.

Holdaway, M. J. (2000). Application of new experimental and garnet Margules data to the garnet-biotite geothermometer. *American mineralogist*, *85*(7-8), 881-892.

Holdsworth, R.E., Harris, A.L. and Roberts, A.M. (1987), The stratigraphy, structure and regional significance of the Moine Rocks of Mull, Argyllshire, W. Scotland. *Geological Journal*., 22, 83-107. https://doi.org/10.1002/gj.3350220203

Holland, T. J. AX: a program to calculate activities of mineral end-members from chemical analyses (Univ. Cambridge, 2009); https://filedn.com/lU1GlyFhv3UuXg5E9dbnWFF/TJBHpages/ax.html

Holland, T., & Blundy, J. (1994). Non-ideal interactions in calcic amphiboles and their bearing on amphibole-plagioclase thermometry. *Contributions to mineralogy and petrology*, 116, 433-447.

Holland, T. J. B & Powell, R. (2011). An improved and extended internally consistent thermodynamic dataset for phases of petrological interest, involving a new equation of state for solids. *Journal of Metamorphic Geology*, 29, 333-383.

Holland, T. J. B., Green, E. C. R., & Powell, R. (2021). A thermodynamic model for feldspars in KAlSi3O8-NaAlSi3O8-CaAl2Si2O8 for mineral equilibrium calculations. *Journal of Metamorphic Geology*, 1-14. doi:10.1111/jmg.12639

Howie, R. A., Zussman, J. & Deer, W., (1992). *An Introduction to the Rock-Forming Minerals* (Longman, 1992).

Holland, T., & Blundy, J. (1994). Non-ideal interactions in calcic amphiboles and their bearing on amphibole-plagioclase thermometry. *Contributions to mineralogy and petrology*, 116, 433-447.

Johnson, T. E., Kirkland, C. L., Viete, D. R., Fischer, S., Reddy, S. M., Evans, N. J., & McDonald, B. J. (2017). Zircon geochronology reveals polyphase magmatism and crustal anatexis in the Buchan Block, NE Scotland: implications for the Grampian Orogeny. *Geoscience Frontiers*, *8*(6), 1469-1478.

Kinny, P. D., Friend, C. R. L., Strachan, R. A., Watt, G. R., & Burns, I. M. (1999). U–Pb geochronology of regional migmatites in East Sutherland, Scotland: evidence for crustal melting during the Caledonian orogeny. *Journal of the Geological Society*, 156(6), 1143-1152.

Kohn, M. J., & Spear, F. (2000). Retrograde net transfer reaction insurance for pressure-temperature estimates. *Geology*, *28*(12), 1127-1130.

Krabbendam, M., Strachan, R., & Prave, T. (2022). A new stratigraphic framework for the early Neoproterozoic successions of Scotland. *Journal of the Geological Society,* 179(2), jgs2021-054.

Lambert, R. J., and McKerrow, W. S. (1976). The Grampian Orogeny. *Scottish Journal of Geology*, 12, 271–92.

Law, R. D., Strachan, R., Thirlwall, M., & Thigpen, J. R. (2024). The Caledonian Orogeny: Late Ordovician–Early Devonian tectonic and magmatic events associated with closure of the Iapetus Ocean. In: Smith, M. & Strachan, R.A. (eds) The Geology of Scotland, *Geological Society, London*, 205-257.

Lamont, T. N., Loader, M. A., Roberts, N. M., Cooper, F. J., Wilkinson, J. J., Bevan, D., Kemp, A., Gorecki, A., Elliott, T., Gardiner, N. J., & Tapster, S. (2024). Porphyry copper formation driven by water-fluxed crustal melting during flat-slab subduction. *Nature Geoscience*, 17, 1306–1315.

Mako, C. A., Law, R. D., Caddick, M. J., Thigpen, J. R., Ashley, K. T., Cottle, J., & Kylander-Clark, A. (2019). Thermal evolution of the Scandian hinterland, Naver nappe, northern Scotland. *Journal of the Geological Society*, 176(4), 669-688.

Mazza, S.E., Mako, C., Law, R.D., Caddick, M.J., Krabbendam, M., Cottle, J. (2018). Thermobarometry of the Moine and Sgurr Beag thrust sheets, northern Scotland, *Journal of Structural Geology*, 113, 10-32, https://doi.org/10.1016/j.jsg.2018.05.002.

Milne, E. J., Neill, I., Bird, A. F., Millar, I. L., McDonald, I., Dempsey, E. D., ... & Waters, E. C. (2023). Caledonian hot zone magmatism in the 'Newer Granites': insight from the Cluanie and Clunes plutons, Northern Scottish Highlands. *Journal of the Geological Society*, *180*(2), jgs2022-076.

Oliver, G. J. H., Chen, F., Buchwaldt, R., & Hegner, E. (2000). Fast tectonometamorphism and exhumation in the type area of the Barrovian and Buchan zones. *Geology*, 28(5), 459-462.

Oliver, G. J., Wilde, S. A., & Wan, Y. (2008). Geochronology and geodynamics of Scottish granitoids from the late Neoproterozoic break-up of Rodinia to Palaeozoic collision. *Journal of the Geological Society*, *165*(3), 661-674.

Pickering, K. T., Bassett, M. G., & Siveter, D. J. (1988). Late Ordovician–early Silurian destruction of the Iapetus Ocean: Newfoundland, British Isles and Scandinavia—a discussion. *Earth and Environmental Science Transactions of the Royal Society of Edinburgh*, 79(4), 361-382.

Searle, M.P. (2021). Tectonic evolution of the Caledonian orogeny in Scotland: a review based on the timing of magmatism, metamorphism and deformation. *Geological Magazine*, https://doi.org/10.1017/S0016756821000947.

Soper, N. T., & Woodcock, N. H. (1990). Silurian collision and sediment dispersal patterns in southern Britain. *Geological Magazine*, 127(6), 527-542.

Soper, N. J., Strachan, R. A., Holdsworth, R. E., Gayer, R. A., & Greiling, R. O. (1992). Sinistral transpression and the Silurian closure of Iapetus. *Journal of the Geological Society*, 149(6), 871-880.

Spear, F.S., (1993). Metamorphic Phase Equilibria and Pressure-Temperature-Time Paths, *Mineralogical Society of America Monograph*, 1, 799.

Strachan, R. A., Alsop, G. I., Ramezani, J., Frazer, R. E., Burns, I. M., & Holdsworth, R. E. (2020). Patterns of Silurian deformation and magmatism during sinistral oblique convergence, northern Scottish Caledonides. *Journal of the Geological Society*, 177(5), 893-910.

Strachan, R., Prave, A. R., Krabbendam, M., & Smith, M. (2024). Late Mesoproterozoic–middle Neoproterozoic: sedimentation and orogeny on the margin of Rodinia. The Geology of Scotland, Martin Smith, Rob Strachan

Vance, D., Strachan, R.A. & Jones, K.A. (1998). Extensional versus compressional settings for metamorphism: Garnet chronometry and pressure-temperature-time histories of the Moine Supergroup, northwest Scotland. *Geology*, 26, 927-930.

Walker, S., Bird, A. F., Thirlwall, M. F., & Strachan, R. A. (2021). Caledonian and Pre-Caledonian orogenic events in Shetland, Scotland: evidence from garnet Lu–Hf and Sm–Nd geochronology. Pannotia to Pangaea: Neoproterozoic and Paleozoic Orogenic Cycles in the Circum-Atlantic Region, J. B. Murphy, R. A. Strachan, C. Quesada.

Weller, O. M., Mottram, C. M., St-Onge, M. R., Möller, C., Strachan, R., Rivers, T., & Copley, A. (2021). The metamorphic and magmatic record of collisional orogens. *Nature Reviews Earth & Environment*, 2(11), 781-799.

Weinberg, R. F., & Hasalová, P. (2015). Water-fluxed melting of the continental crust: A review. *Lithos*, 212, 158-188.

Wheeler, J., Mangon, L. S., Prior, D.J., (2004). Disequilibrium in the Ross of Mull Contact Metamorphic Aureole, Scotland: a Consequence of Polymetamorphism, *Journal of Petrology*, v. 45, p. 835-853, https://doi.org/10.1093/petrology/egg113

White, R. W., Powell, R., Holland, T. J. B., & Worley, B. A. (2000) The effect of TiO2 an Fe2O3 on metapelitic assemblages at greenschist and amphibolite facies conditions: mineral equilibria calculations in the system K2O-FeO-MgO-Al2O3-SiO2-H2O-TiO2-Fe2O3. *Journal of Metamorphic Geology*, 18, 497-511.

White, R. W., Powell, R., & Johnson, T. E. (2014). The effect of Mn on mineral stability in metapelites revisited: New a–x relations for manganese-bearing minerals. *Journal of Metamorphic Geology*, 32(8), 809-828.

Whitney, D. L., & Evans, B. W. (2010). Abbreviations for names of rock-forming minerals. *American mineralogist*, *95*(1), 185-187.

Yonkee, W. A., & Weil, A. B. (2015). Tectonic evolution of the Sevier and Laramide belts within the North American Cordillera orogenic system. *Earth-Science Reviews*, 150, 531-593.

Zaniewski, A., Reavy, R. J., & Harris, A. L. (2006). Field relationships and emplacement of the Caledonian Ross of Mull Granite, Argyllshire. *Scottish Journal of Geology*, *42*(2), 179-189.

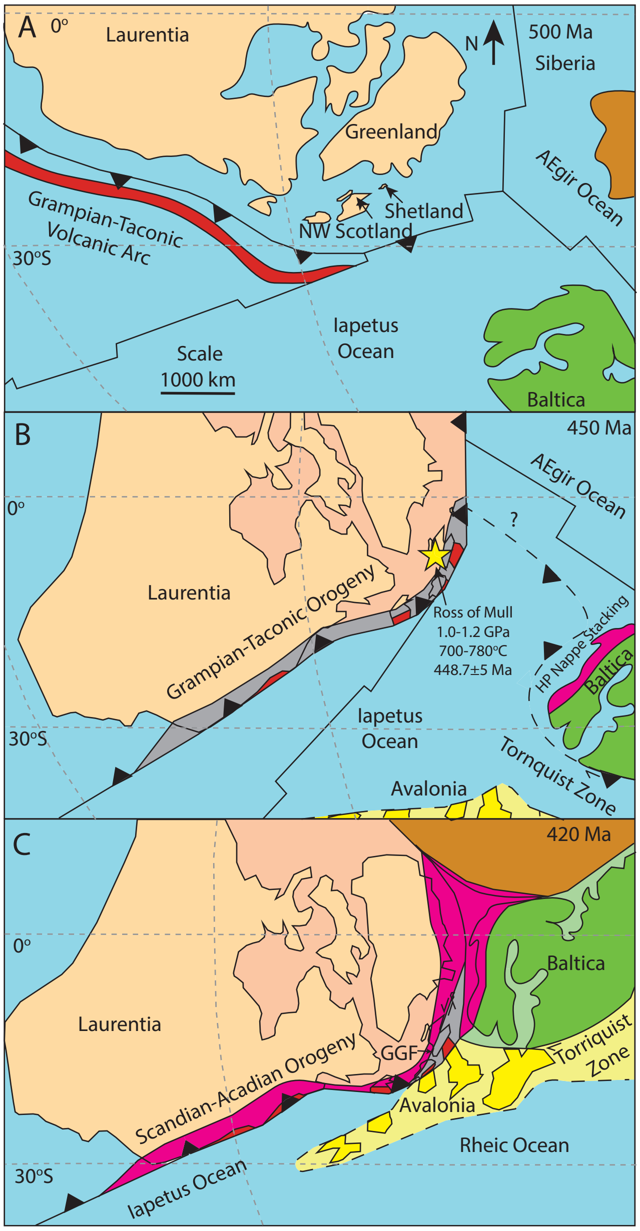
A
0°
Laurentia
N
500 Ma
Siberia
Greenland
AEgir Ocean
Shetland
NW Scotland
Grampian-Taconic Volcanic Arc
30°S
Iapetus Ocean
Scale
1000 km
Baltica
B
450 Ma
AEgir Ocean
0°
?
Laurentia
Grampian-Taconic Orogeny
Ross of Mull
1.0-1.2 GPa
700-780°C
448.7±5 Ma
HP Nappe Stacking
Baltica
Iapetus Ocean
30°S
Tornquist Zone
Avalonia
C
420 Ma
0°
Baltica
Laurentia
Scandian-Acadian Orogeny
GGF
Torriquist Zone
Avalonia
Rheic Ocean
30°S
Iapetus Ocean

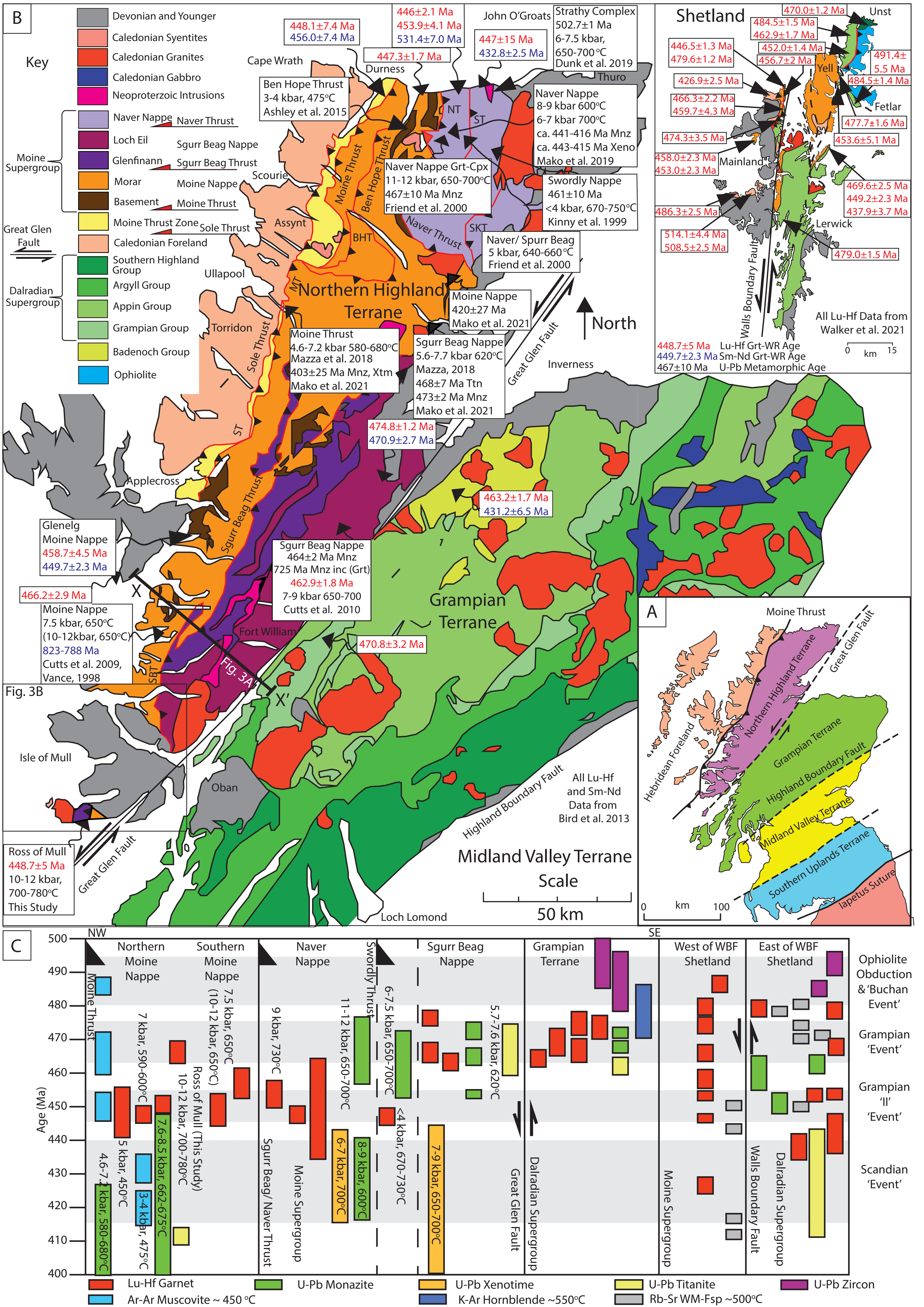
B
Key
Devonian and Younger
Caledonian Syentites
Caledonian Granites
Caledonian Gabbro
Neoproterzoic Intrusions
Moine Supergroup
Naver Nappe
Naver Thrust
Loch Eil
Sgurr Beag Nappe
Glenfinnan
Sgurr Beag Thrust
Morar
Moine Nappe
Basement
Moine Thrust
Moine Thrust Zone
Sole Thrust
Great Glen Fault
Caledonian Foreland
Dalradian Supergroup
Southern Highland Group
Argyll Group
Appin Group
Grampian Group
Badenoch Group
Ophiolite
Cape Wrath
Durness
John O'Groats
Thuro
448.1±7.4 Ma
456.0±7.4 Ma
446±2.1 Ma
453.9±4.1 Ma
531.4±7.0 Ma
447.3±1.7 Ma
447±15 Ma
432.8±2.5 Ma
Strathy Complex
502.7±1 Ma
6-7.5 kbar,
650-700 °C
Dunk et al. 2019
Ben Hope Thrust
3-4 kbar, 475°C
Ashley et al. 2015
Naver Nappe
8-9 kbar 600°C
6-7 kbar 700°C
ca. 441-416 Ma Mnz
ca. 443-415 Ma Xeno
Mako et al. 2019
NT
ST
Scourie
Moine Thrust
Ben Hope Thrust
Naver Nappe Grt-Cpx
11-12 kbar, 650-700°C
467±10 Ma Mnz
Friend et al. 2000
Swordly Nappe
461±10 Ma
<4 kbar, 670-750°C
Kinny et al. 1999
Assynt
BHT
Naver Thrust
SKT
Naver/ Spurr Beag
5 kbar, 640-660°C
Friend et al. 2000
Ullapool
MT
Northern Highland Terrane
Moine Nappe
420±27 Ma
Mako et al. 2021
North
Torridon
Sole Thrust
Moine Thrust
4.6-7.2 kbar 580-680°C
Mazza et al. 2018
403±25 Ma Mnz, Xtm
Mako et al. 2021
Sgurr Beag Nappe
5.6-7.7 kbar 620°C
Mazza, 2018
468±7 Ma Ttn
473±2 Ma Mnz
Mako et al. 2021
Great Glen Fault
Inverness
ST
474.8±1.2 Ma
470.9±2.7 Ma
Applecross
Sgurr Beag Thrust
463.2±1.7 Ma
431.2±6.5 Ma
Glenelg
Moine Nappe
458.7±4.5 Ma
449.7±2.3 Ma
Sgurr Beag Nappe
464±2 Ma Mnz
725 Ma Mnz inc (Grt)
462.9±1.8 Ma
7-9 kbar 650-700
Cutts et al. 2010
X
466.2±2.9 Ma
Moine Nappe
7.5 kbar, 650°C
(10-12kbar, 650°C)
823-788 Ma
Cutts et al. 2009,
Vance, 1998
Grampian Terrane
Fort William
Fig. 3A
470.8±3.2 Ma
SBT
X'
Fig. 3B
Isle of Mull
Oban
All Lu-Hf and Sm-Nd Data from Bird et al. 2013
Highland Boundary Fault
Ross of Mull
448.7±5 Ma
10-12 kbar,
700-780°C
This Study
Great Glen Fault
Midland Valley Terrane
Scale
50 km
Loch Lomond
Shetland
470.0±1.2 Ma
Unst
484.5±1.5 Ma
462.9±1.7 Ma
446.5±1.3 Ma
479.6±1.2 Ma
452.0±1.4 Ma
456.7±2 Ma
Yell
491.4±5.5 Ma
484.5±1.4 Ma
426.9±2.5 Ma
466.3±2.2 Ma
459.7±4.3 Ma
Fetlar
477.7±1.6 Ma
474.3±3.5 Ma
453.6±5.1 Ma
458.0±2.3 Ma
453.0±2.3 Ma
Mainland
469.6±2.5 Ma
449.2±2.3 Ma
437.9±3.7 Ma
486.3±2.5 Ma
Lerwick
514.1±4.4 Ma
508.5±2.5 Ma
479.0±1.5 Ma
Walls Boundary Fault
All Lu-Hf Data from Walker et al. 2021
0 km 15
448.7±5 Ma Lu-Hf Grt-WR Age
449.7±2.3 Ma Sm-Nd Grt-WR Age
467±10 Ma U-Pb Metamorphic Age
A
Moine Thrust
Great Glen Fault
Northern Highland Terrane
Hebridean Foreland
Grampian Terrane
Highland Boundary Fault
Midland Valley Terrane
Southern Uplands Terrane
Iapetus Suture
0 km 100
C
NW
SE
Northern Moine Nappe
Southern Moine Nappe
Naver Nappe
Swordly Thrust
Sgurr Beag Nappe
Grampian Terrane
West of WBF Shetland
East of WBF Shetland
Age (Ma)
500
490
480
470
460
450
440
430
420
410
400
Moine Thrust
7 kbar, 590-600°C
5 kbar, 450°C
4.6-7.2 kbar, 580-680°C
3-4 kbar, 475°C
7.6-8.5 kbar, 662-675°C
10-12 kbar, 700-780°C
Ross of Mull (This Study)
7.5 kbar, 650°C
(10-12 kbar, 650°C)
9 kbar, 730°C
Sgurr Beag/ Naver Thrust
Moine Supergroup
11-12 kbar, 650-700°C
6-7 kbar, 700°C
8-9 kbar, 600°C
6-7.5 kbar, 650-700°C
<4 kbar, 670-730°C
7-9 kbar, 650-700°C
5.7-7.6 kbar, 620°C
Great Glen Fault
Dalradian Supergroup
Moine Supergroup
Walls Boundary Fault
Dalradian Supergroup
Ophiolite Obduction & 'Buchan Event'
Grampian 'Event'
Grampian 'II' 'Event'
Scandian 'Event'
Lu-Hf Garnet
U-Pb Monazite
U-Pb Xenotime
U-Pb Titanite
U-Pb Zircon
Ar-Ar Muscovite ~ 450 °C
K-Ar Hornblende ~550°C
Rb-Sr WM-Fsp ~500°C

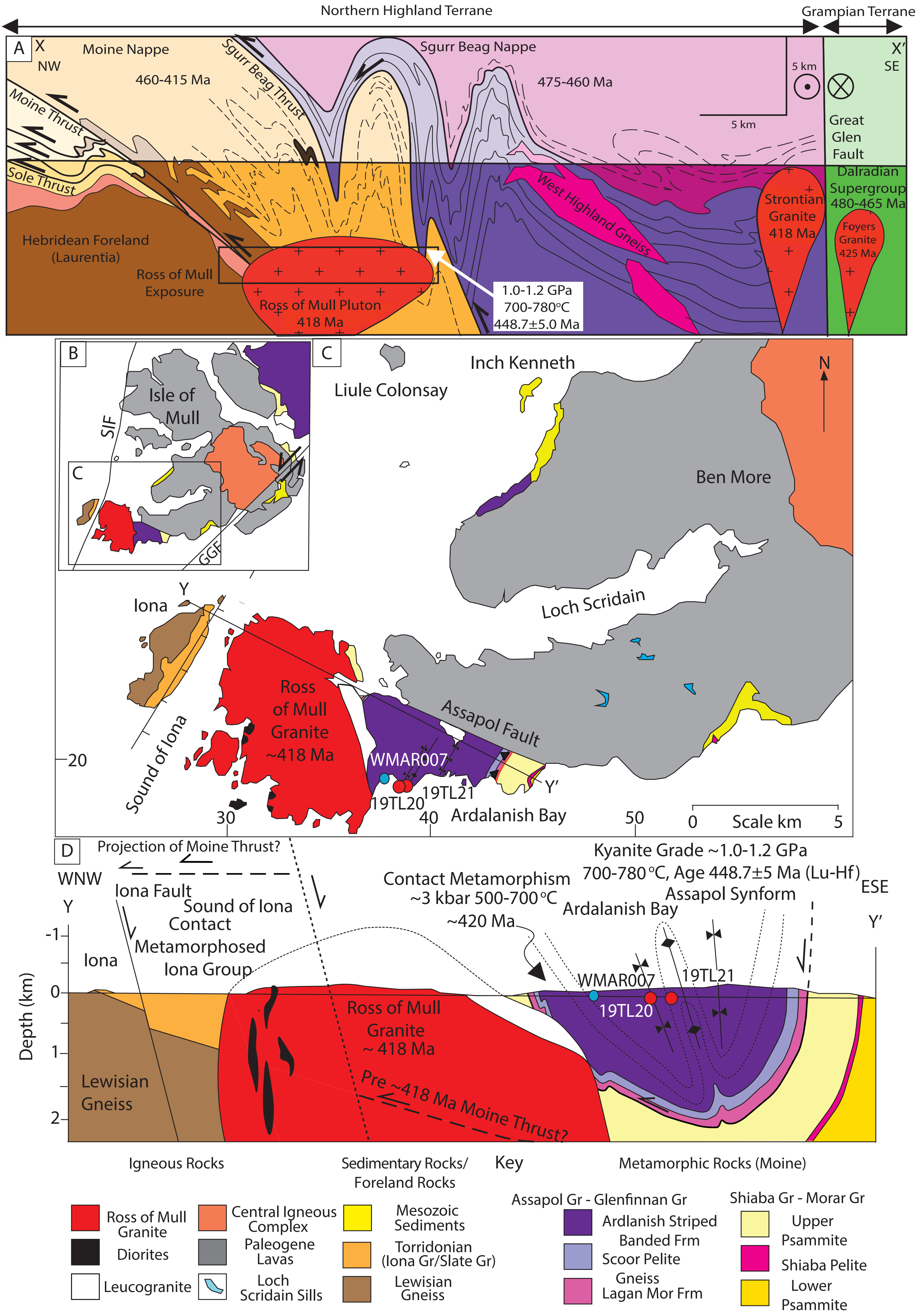
Northern Highland Terrane
Grampian Terrane
A
X
NW
X'
SE
Moine Nappe
460-415 Ma
Sgurr Beag Thrust
Sgurr Beag Nappe
475-460 Ma
Moine Thrust
Sole Thrust
5 km
5 km
Great Glen Fault
Dalradian Supergroup 480-465 Ma
Strontian Granite 418 Ma
Foyers Granite 425 Ma
West Highland Gneiss
Hebridean Foreland (Laurentia)
Ross of Mull Exposure
Ross of Mull Pluton 418 Ma
1.0-1.2 GPa
700-780°C
448.7±5.0 Ma
B
Isle of Mull
SIF
C
GGF
Liule Colonsay
Inch Kenneth
N
Ben More
Loch Scridain
Iona
Y
Y'
Ross of Mull Granite ~418 Ma
Sound of Iona
Assapol Fault
WMAR007
19TL20
19TL21
Ardalanish Bay
20
30
40
50
0
Scale km
5
D
Projection of Moine Thrust?
WNW
ESE
Iona Fault
Sound of Iona Contact Metamorphosed Iona Group
Iona
Contact Metamorphism ~3 kbar 500-700 °C ~420 Ma
Kyanite Grade ~1.0-1.2 GPa 700-780 °C, Age 448.7±5 Ma (Lu-Hf)
Assapol Synform
Ardalanish Bay
Depth (km)
-1
0
1
2
Lewisian Gneiss
Ross of Mull Granite ~ 418 Ma
Pre ~418 Ma Moine Thrust?
Key
Igneous Rocks
Ross of Mull Granite
Diorites
Leucogranite
Central Igneous Complex
Paleogene Lavas
Loch Scridain Sills
Sedimentary Rocks/ Foreland Rocks
Mesozoic Sediments
Torridonian (Iona Gr/Slate Gr)
Lewisian Gneiss
Metamorphic Rocks (Moine)
Assapol Gr - Glenfinnan Gr
Ardlanish Striped Banded Frm
Scoor Pelite Gneiss
Lagan Mor Frm
Shiaba Gr - Morar Gr
Upper Psammite
Shiaba Pelite
Lower Psammite

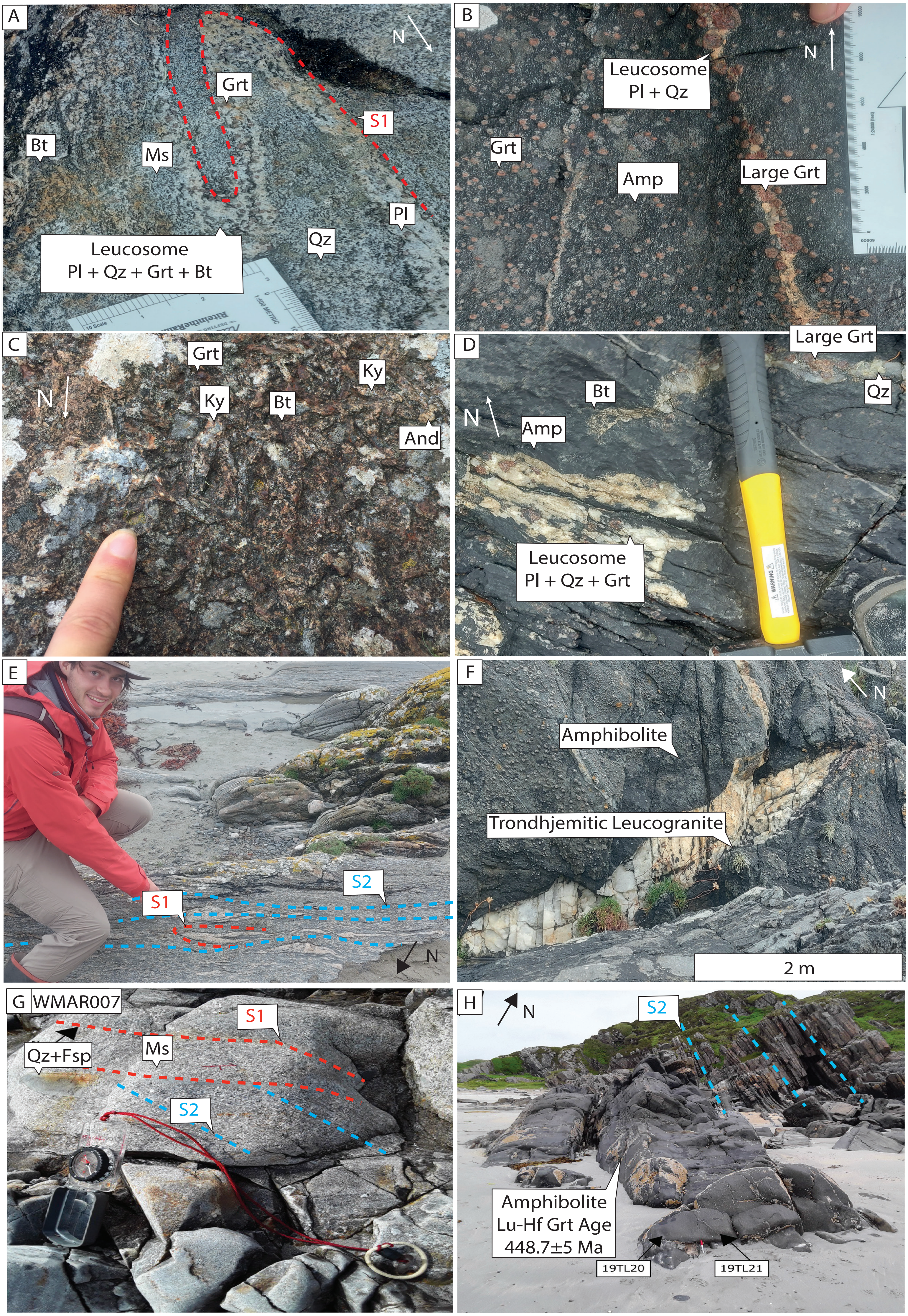

A
N
Grt
S1
Bt
Ms
Pl
Qz
Leucosome
Pl + Qz + Grt + Bt
B
Leucosome
Pl + Qz
N
Grt
Amp
Large Grt
C
Grt
Ky
N
Ky
Bt
And
D
Large Grt
Bt
Qz
N
Amp
Leucosome
Pl + Qz + Grt
E
S2
S1
N
F
N
Amphibolite
Trondhjemitic Leucogranite
2 m
G
WMAR007
S1
Ms
Qz+Fsp
S2
H
N
S2
Amphibolite
Lu-Hf Grt Age
448.7±5 Ma
19TL20
19TL21

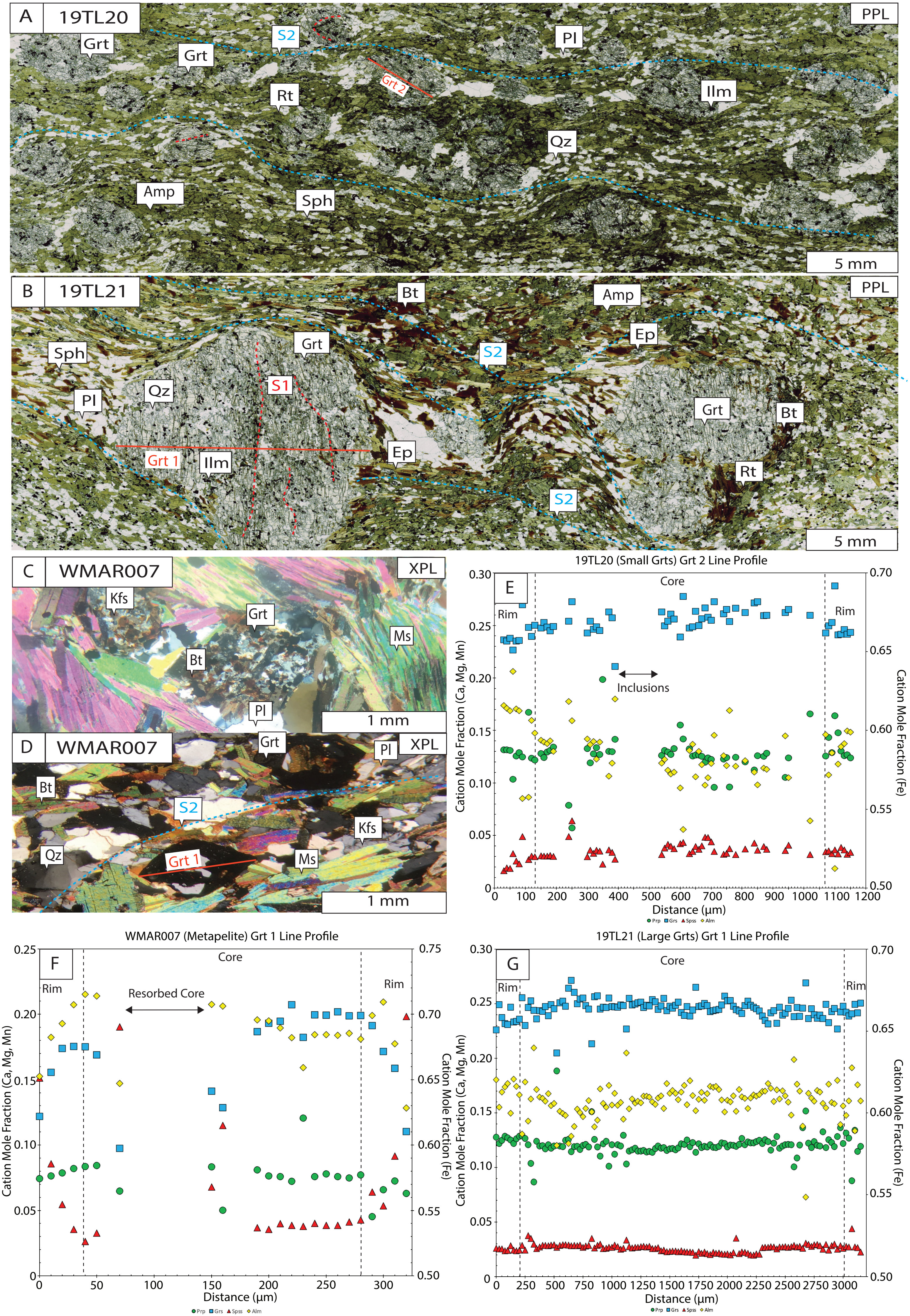

A
19TL20
PPL
Grt
Grt
S2
Pl
Grt 2
Rt
Ilm
Qz
Amp
Sph
5 mm
B
19TL21
PPL
Bt
Amp
Sph
Grt
Ep
S2
S1
Qz
Pl
Grt
Bt
Grt 1
Ilm
Ep
Rt
S2
5 mm
C
WMAR007
XPL
Kfs
Grt
Ms
Bt
Pl
1 mm
D
WMAR007
XPL
Grt
Pl
Bt
S2
Kfs
Qz
Grt 1
Ms
1 mm
19TL20 (Small Grts) Grt 2 Line Profile
E
Core
Rim
Rim
Inclusions
Cation Mole Fraction (Ca, Mg, Mn)
Cation Mole Fraction (Fe)
Distance (µm)
Prp Grs Spss Alm
WMAR007 (Metapelite) Grt 1 Line Profile
F
Core
Rim
Rim
Resorbed Core
Cation Mole Fraction (Ca, Mg, Mn)
Cation Mole Fraction (Fe)
Distance (µm)
Prp Grs Spss Alm
19TL21 (Large Grts) Grt 1 Line Profile
G
Core
Rim
Rim
Cation Mole Fraction (Ca, Mg, Mn)
Cation Mole Fraction (Fe)
Distance (µm)
Prp Grs Spss Alm

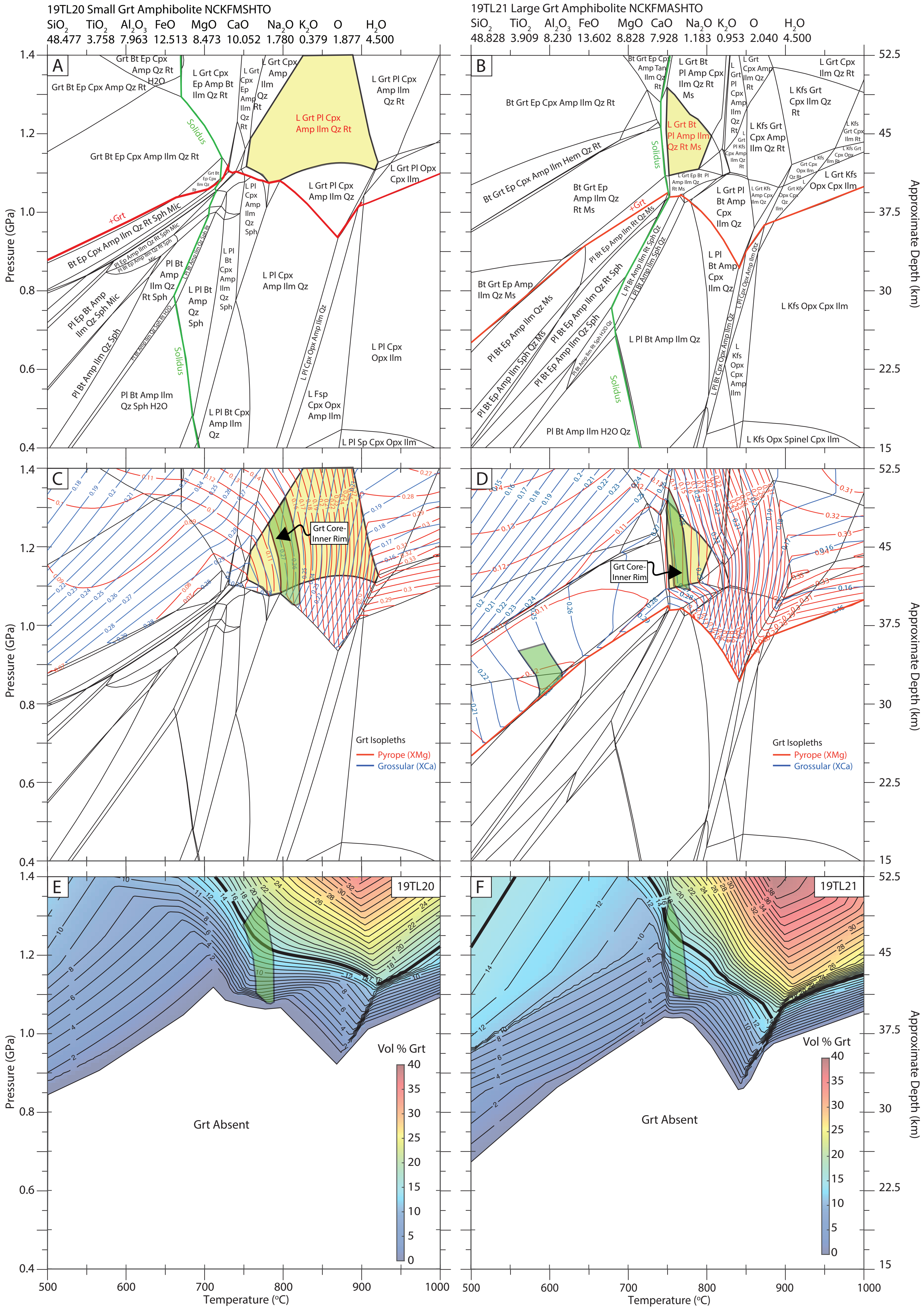

19TL20 Small Grt Amphibolite NCKFMSHTO
SiO2 TiO2 Al2O3 FeO MgO CaO Na2O K2O O H2O
48.477 3.758 7.963 12.513 8.473 10.052 1.780 0.379 1.877 4.500
19TL21 Large Grt Amphibolite NCKFMASHTO
SiO2 TiO2 Al2O3 FeO MgO CaO Na2O K2O O H2O
48.828 3.909 8.230 13.602 8.828 7.928 1.183 0.953 2.040 4.500
A
Grt Bt Ep Cpx Amp Qz Rt
Grt Bt Ep Cpx Amp Qz Rt H2O
L Grt Cpx Ep Amp Bt Ilm Qz Rt
L Grt Cpx Amp Ilm Qz
L Grt Pl Cpx Amp Ilm Qz Rt
L Grt Pl Cpx Amp Ilm Qz Rt
Solidus
Grt Bt Ep Cpx Amp Ilm Qz Rt
L Grt Pl Opx Cpx Ilm
L Grt Pl Cpx Amp Ilm Qz
+Grt
Bt Ep Cpx Amp Ilm Qz Rt Sph Mic
Pl Bt Amp Ilm Qz Rt Sph
L Pl Bt Amp Qz Sph
L Pl Cpx Amp Ilm Qz Sph
L Pl Cpx Amp Ilm Qz
Pl Ep Bt Amp Ilm Qz Sph Mic
Pl Bt Amp Ilm Qz Sph
Pl Bt Amp Ilm Qz Sph H2O
L Pl Cpx Opx Amp Ilm Qz
L Pl Cpx Opx Ilm
L Fsp Cpx Opx Amp Ilm
L Pl Bt Cpx Amp Ilm Qz
L Pl Sp Cpx Opx Ilm
B
Bt Grt Ep Cpx Amp Ilm Qz Rt
L Grt Bt Pl Amp Cpx Ilm Qz Rt Ms
L Grt Cpx Ilm Qz Rt
L Kfs Grt Cpx Ilm Qz Rt
L Grt Bt Pl Amp Ilm Qz Rt Ms
L Kfs Grt Cpx Amp Ilm Qz Rt
Bt Grt Ep Cpx Amp Ilm Hem Qz Rt
Bt Grt Ep Amp Ilm Qz Rt Ms
L Grt Pl Bt Amp Cpx Ilm Qz
L Grt Kfs Opx Cpx Ilm
+Grt
Bt Grt Ep Amp Ilm Qz Ms
Pl Bt Ep Amp Ilm Qz Ms
L Pl Bt Amp Ilm Qz
L Kfs Opx Cpx Ilm
L Kfs Opx Cpx Amp Ilm
Pl Bt Amp Ilm H2O Qz
L Kfs Opx Spinel Cpx Ilm
C
Grt Core-Inner Rim
Grt Isopleths
Pyrope (XMg)
Grossular (XCa)
D
Grt Core-Inner Rim
Grt Isopleths
Pyrope (XMg)
Grossular (XCa)
E
19TL20
Vol % Grt
Grt Absent
F
19TL21
Vol % Grt
Grt Absent
Pressure (GPa)
Temperature (°C)
Approximate Depth (km)

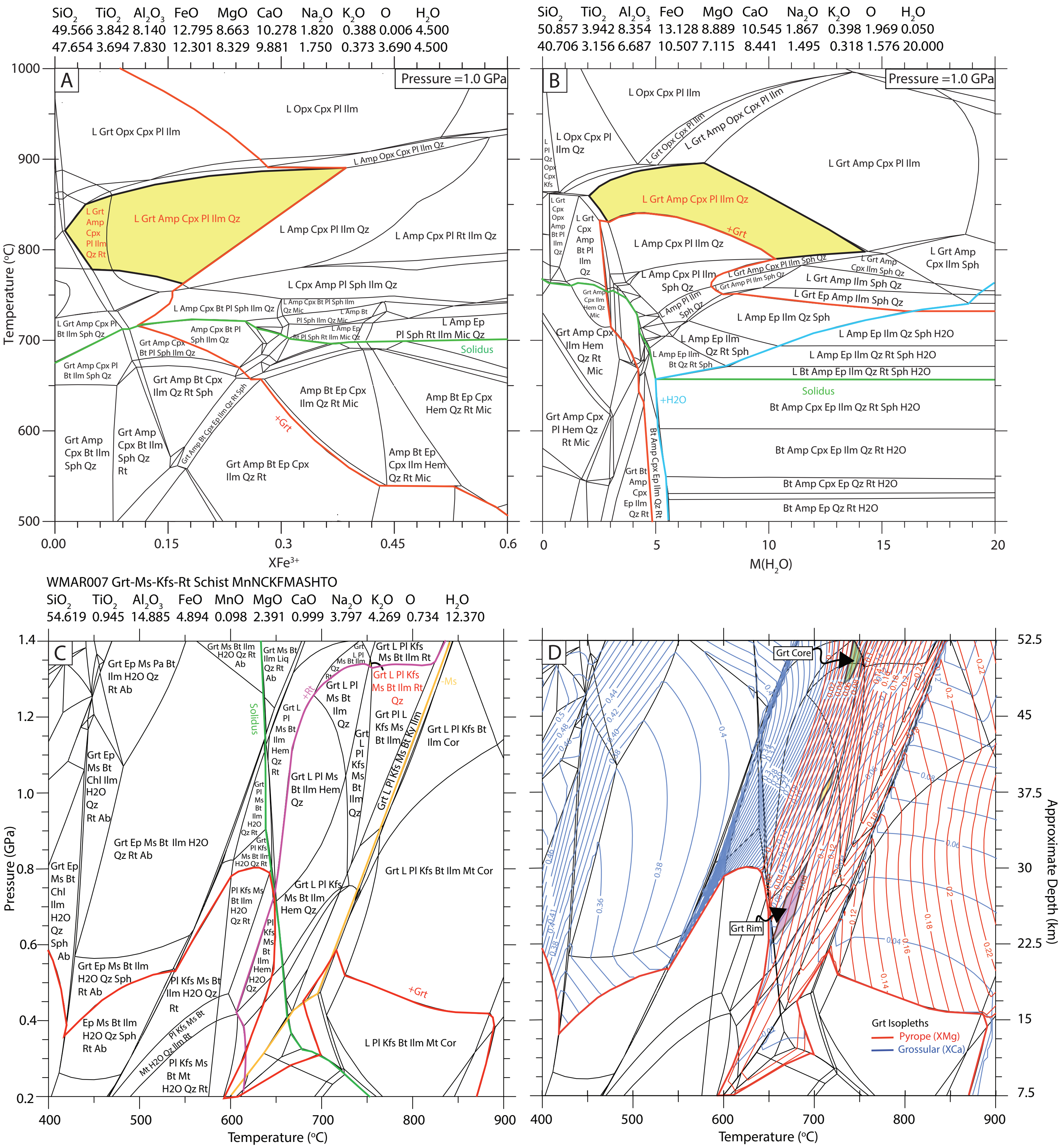
SiO2 TiO2 Al2O3 FeO MgO CaO Na2O K2O O H2O
49.566 3.842 8.140 12.795 8.663 10.278 1.820 0.388 0.006 4.500
47.654 3.694 7.830 12.301 8.329 9.881 1.750 0.373 3.690 4.500
A
Pressure =1.0 GPa
L Opx Cpx Pl Ilm
L Grt Opx Cpx Pl Ilm
L Amp Opx Cpx Pl Ilm Qz
L Grt Amp Cpx Pl Ilm Qz Rt
L Grt Amp Cpx Pl Ilm Qz
L Amp Cpx Pl Ilm Qz
L Amp Cpx Pl Rt Ilm Qz
L Cpx Amp Pl Sph Ilm Qz
L Amp Cpx Bt Pl Sph Ilm Qz
L Grt Amp Cpx Pl Bt Ilm Sph Qz
Amp Cpx Bt Pl Sph Ilm Qz
Grt Amp Cpx Bt Pl Sph Ilm Qz
L Amp Ep Pl Sph Rt Ilm Mic Qz
Solidus
Grt Amp Cpx Pl Bt Ilm Sph Qz
Grt Amp Bt Cpx Ilm Qz Rt Sph
Amp Bt Ep Cpx Ilm Qz Rt Mic
Amp Bt Ep Cpx Hem Qz Rt Mic
+Grt
Grt Amp Cpx Bt Ilm Sph Qz
Grt Amp Cpx Bt Ilm Sph Qz Rt
Grt Amp Bt Cpx Ep Ilm Qz Rt Sph
Grt Amp Bt Ep Cpx Ilm Qz Rt
Amp Bt Ep Cpx Ilm Hem Qz Rt Mic
Temperature (°C)
XFe3+
SiO2 TiO2 Al2O3 FeO MgO CaO Na2O K2O O H2O
50.857 3.942 8.354 13.128 8.889 10.545 1.867 0.398 1.969 0.050
40.706 3.156 6.687 10.507 7.115 8.441 1.495 0.318 1.576 20.000
B
Pressure =1.0 GPa
L Opx Cpx Pl Ilm
L Opx Cpx Pl Ilm Qz
L Grt Opx Cpx Pl Ilm
L Grt Amp Opx Cpx Pl Ilm
L Grt Amp Cpx Pl Ilm
L Grt Amp Cpx Pl Ilm Qz
+Grt
L Amp Cpx Pl Ilm Qz
L Grt Amp Cpx Ilm Sph
L Amp Cpx Pl Ilm Sph Qz
L Grt Amp Ilm Sph Qz
L Grt Ep Amp Ilm Sph Qz
L Amp Ep Ilm Qz Sph
L Amp Ep Ilm Qz Sph H2O
L Amp Ep Ilm Qz Rt Sph H2O
L Bt Amp Ep Ilm Qz Rt Sph H2O
Solidus
+H2O
Bt Amp Cpx Ep Ilm Qz Rt Sph H2O
Bt Amp Cpx Ep Ilm Qz Rt H2O
Bt Amp Cpx Ep Qz Rt H2O
Bt Amp Ep Qz Rt H2O
Grt Amp Cpx Ilm Hem Qz Rt Mic
Grt Amp Cpx Pl Hem Qz Rt Mic
Bt Amp Cpx Ep Ilm Qz Rt
M(H2O)
WMAR007 Grt-Ms-Kfs-Rt Schist MnNCKFMASHTO
SiO2 TiO2 Al2O3 FeO MnO MgO CaO Na2O K2O O H2O
54.619 0.945 14.885 4.894 0.098 2.391 0.999 3.797 4.269 0.734 12.370
C
Grt Ep Ms Pa Bt Ilm H2O Qz Rt Ab
Grt Ep Ms Bt Chl Ilm H2O Qz Rt Ab
Grt Ep Ms Bt Ilm H2O Qz Rt Ab
Solidus
Grt L Pl Kfs Ms Bt Ilm Rt
Grt L Pl Kfs Ms Bt Ilm Rt Qz
-Ms
+Rt
Grt L Pl Kfs Bt Ilm Cor
Grt L Pl Kfs Bt Ilm Mt Cor
Grt L Pl Kfs Ms Bt Ilm Hem Qz
Grt L Pl Ms Bt Ilm Hem Qz
Grt Ep Ms Bt Ilm H2O Qz Sph Rt Ab
Ep Ms Bt Ilm H2O Qz Sph Rt Ab
Pl Kfs Ms Bt Ilm H2O Qz Rt
Pl Kfs Ms Bt Mt H2O Qz Rt
+Grt
L Pl Kfs Bt Ilm Mt Cor
Pressure (GPa)
Temperature (°C)
D
Grt Core
Grt Rim
Grt Isopleths
Pyrope (XMg)
Grossular (XCa)
Approximate Depth (km)

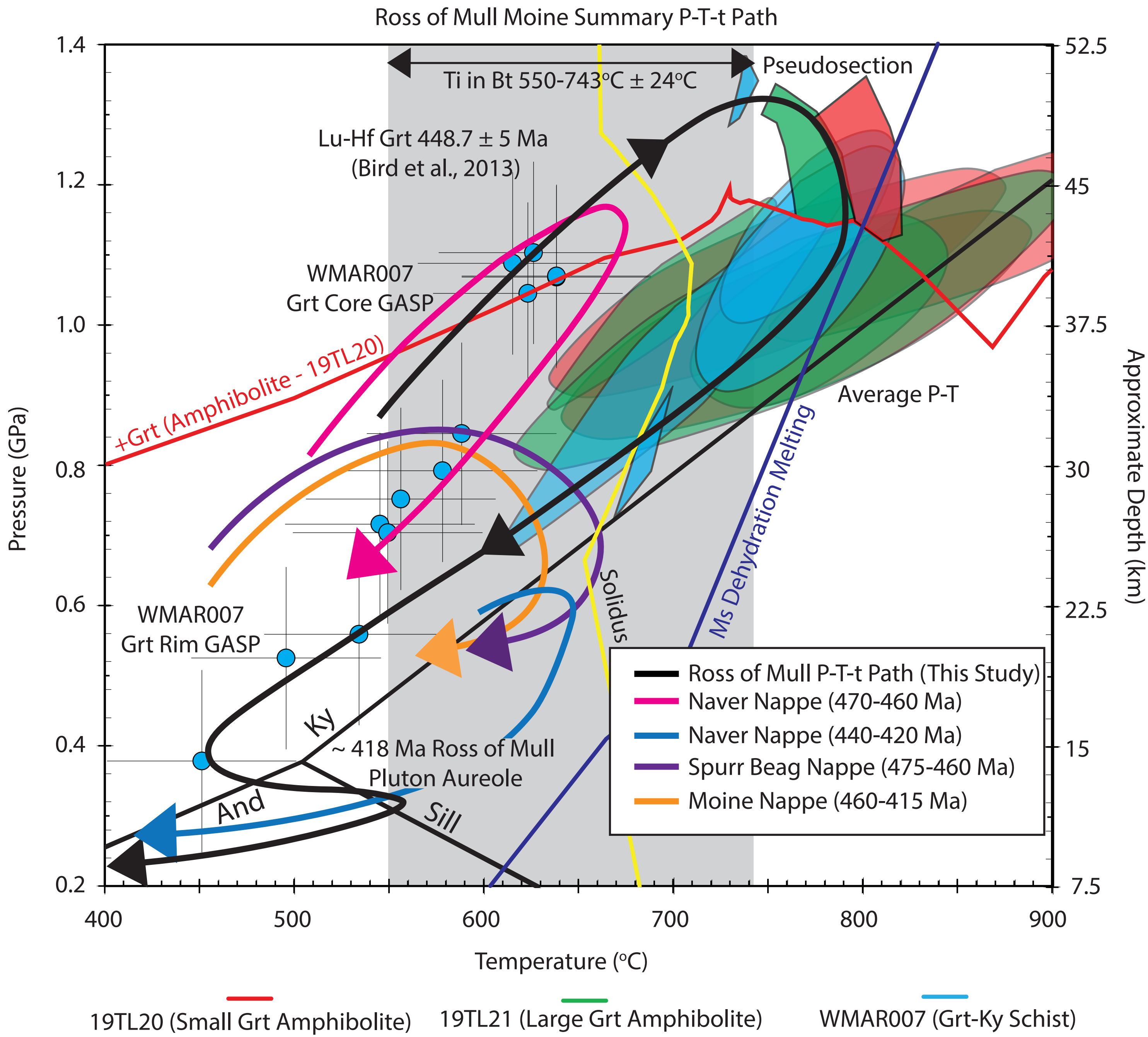
Ross of Mull Moine Summary P-T-t Path
Ti in Bt 550-743°C ± 24°C
Pseudosection
Lu-Hf Grt 448.7 ± 5 Ma
(Bird et al., 2013)
WMAR007
Grt Core GASP
+Grt (Amphibolite - 19TL20)
Average P-T
Ms Dehydration Melting
Solidus
WMAR007
Grt Rim GASP
Ky
~ 418 Ma Ross of Mull
Pluton Aureole
And
Sill
Ross of Mull P-T-t Path (This Study)
Naver Nappe (470-460 Ma)
Naver Nappe (440-420 Ma)
Spurr Beag Nappe (475-460 Ma)
Moine Nappe (460-415 Ma)
Pressure (GPa)
Approximate Depth (km)
Temperature (°C)
1.4
1.2
1.0
0.8
0.6
0.4
0.2
52.5
45
37.5
30
22.5
15
7.5
400
500
600
700
800
900
19TL20 (Small Grt Amphibolite)
19TL21 (Large Grt Amphibolite)
WMAR007 (Grt-Ky Schist)

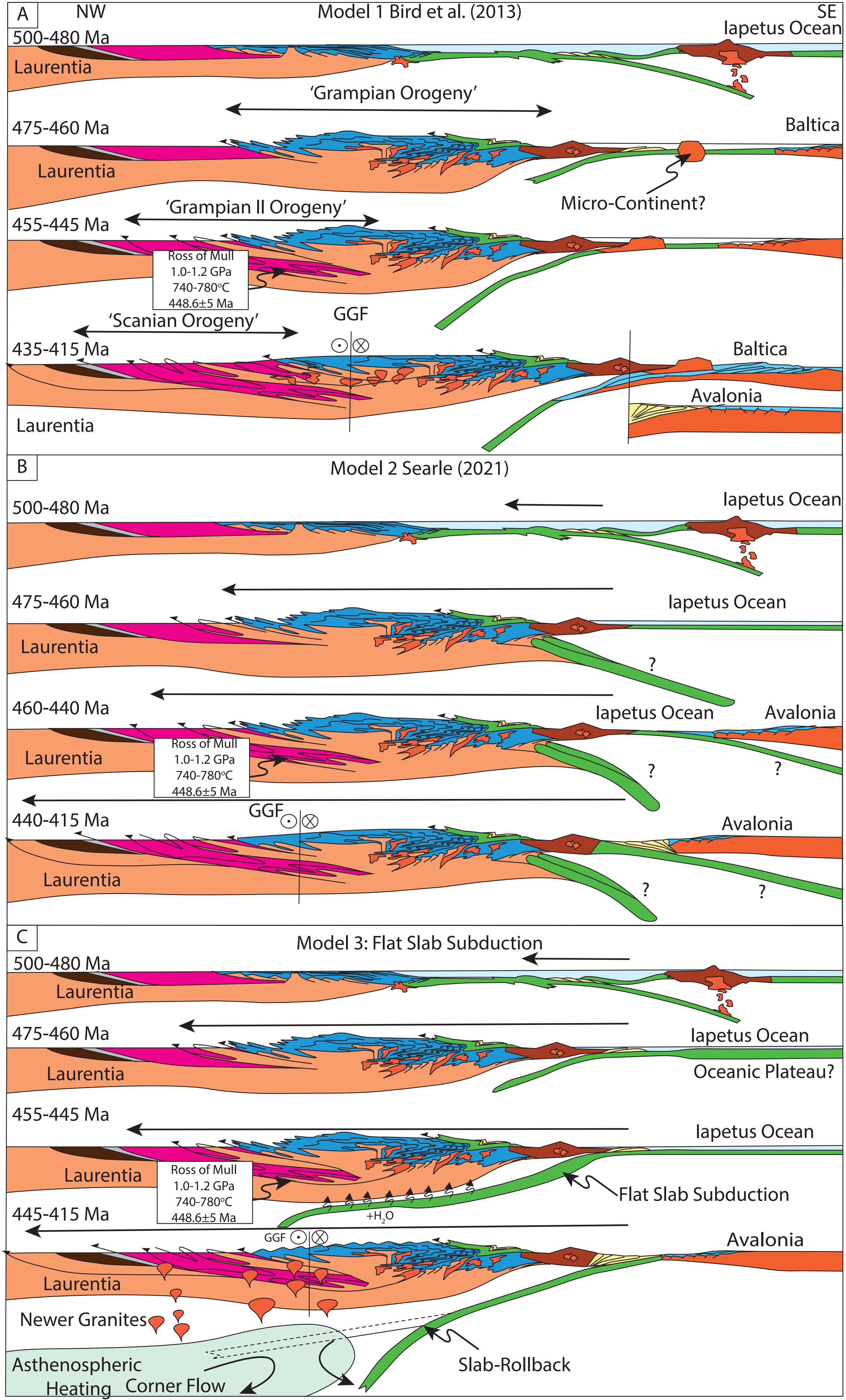

A
NW
Model 1 Bird et al. (2013)
SE
Iapetus Ocean
500-480 Ma
Laurentia
'Grampian Orogeny'
475-460 Ma
Baltica
Laurentia
Micro-Continent?
'Grampian II Orogeny'
455-445 Ma
Ross of Mull
1.0-1.2 GPa
740-780°C
448.6±5 Ma
'Scanian Orogeny'
GGF
435-415 Ma
Baltica
Avalonia
Laurentia
B
Model 2 Searle (2021)
500-480 Ma
Iapetus Ocean
475-460 Ma
Iapetus Ocean
Laurentia
?
460-440 Ma
Iapetus Ocean
Avalonia
Laurentia
Ross of Mull
1.0-1.2 GPa
740-780°C
448.6±5 Ma
?
?
440-415 Ma
GGF
Avalonia
Laurentia
?
?
C
Model 3: Flat Slab Subduction
500-480 Ma
Laurentia
475-460 Ma
Iapetus Ocean
Laurentia
Oceanic Plateau?
455-445 Ma
Iapetus Ocean
Laurentia
Ross of Mull
1.0-1.2 GPa
740-780°C
448.6±5 Ma
Flat Slab Subduction
+H$_2$O
445-415 Ma
GGF
Avalonia
Laurentia
Newer Granites
Asthenospheric
Heating
Corner Flow
Slab-Rollback

Table 1

Sample	Method	Temperature (°C)	Pressure (GPa)	Notes
19TL21	Amphibole-Plagioclase (H&B, 1994)	671 ± 15 (Edenite-Tremolite)	-	Based on matrix plagioclase (An = 0.28)
	Amphibole-Plagioclase (H&B, 1994)	688 ± 21 (Edenite-Richterite)	-	
	Ti-in-Biotite (Henry et al., 2005)	723 ± 12	-	Most biotite clusters 660-670°C, retrograde
	THERMOCALC (H&P, 2011)	777 ± 54	1.02 ± 0.11	Based on Grt-Amp-Bt-Fsp-Rt-Ilm-Ep-Qz-Sph-H_2O assemblage
	Phase Diagram (Pseudosection)	760–780	1.08–1.30	Garnet isopleths (XPrp 0.13, XGrs 0.26), 15% garnet volume
19TL20	Amphibole-Plagioclase (H&B, 1994)	665 ± 15 (Edenite-Tremolite)	-	
	Amphibole-Plagioclase (H&B, 1994)	717 ± 34 (Edenite-Richterite)	-	
	THERMOCALC (H&P, 2011)	755 ± 96	1.06 ± 0.13	Based on Grt-Amp-Fsp-Rt-Ilm-Qz-Sph-H_2O assemblage
	Phase Diagram (Pseudosection)	790–810	1.05–1.30	Garnet isopleths (XPrp 0.13, XGrs 0.26), 15% garnet volume
WMAR007	Ti-in-Biotite (Henry et al., 2005)	748 ± 12	-	
	Garnet-Biotite (B, 1992) + GASP/GPMB Barometry (S, 1993)	638 ± 30	1.28 (GPMB_Mg), 1.04 (GPMB_Fe), 1.07 (GASP) ± 0.12	Garnet core conditions
	Garnet Rim (Retrograde)	496 ± 30	0.53 (GASP), 0.67 (GPMB_Mg), 0.51 (GPMB_Fe) ± 0.12	Garnet in contact with biotite
	THERMOCALC (H&P, 2011)	750 ± 41	1.06 ± 0.14	Based on Grt-Ms-Bt-Kfs-Fsp-Qz-Rt-Ilm-H_2O assemblage
	Phase Diagram (Pseudosection)	720–750	1.2–1.3	Garnet core isopleths (XPrp 0.08, XGrs 0.20)